THE ASTROPHYSICAL JOURNAL SUPPLEMENT SERIES, 105:299–330, 1996 August

VLBA OBSERVATIONS OF RADIO REFERENCE FRAME SOURCES. I.

ALAN L. FEY
US Naval Observatory, Code EO, 3450 Massachusetts Ave NW, Washington, DC 20392-5420; afey@alf.usno.navy.mil
ANDREW W. CLEGG
Naval Research Laboratory, Code 7213, Washington, DC 20375-5351; clegg@funafuti.nrl.navy.mil
AND
EDWARD B. FOMALONT
National Radio Astronomy Observatory, 520 Edgemont Road, Charlottesville, VA 22903-2475; efomalon@nrao.edu
Received 1995 October 13; accepted 1996 February 1

ABSTRACT

We present first-epoch simultaneous dual-frequency VLBA 2 GHz and 8 GHz observations of a sample of 42 of the 560 extragalactic sources for which positions were reported by Johnston et al. Many of the observed sources have dominant cores containing the majority of the total flux density and angular sizes less than several milliarcseconds. However, at some level, almost all the observed sources show structure characteristic of a core-jet morphology, often with multiple jet components. Analysis of source structure corrections to the measured VLBI group delay, based on the images presented here, confirm that intrinsic structure contributions can be significant. These observations represent the first in a series of observations intended to image the entire set of sources presented by Johnston et al.

Subject headings: galaxies: jets — galaxies: structure — radio continuum: galaxies

1. INTRODUCTION

Many of the most intense compact extragalactic radio sources are used routinely to determine tectonic plate motion to accuracies on the order of several millimeters, to determine Earth rotation parameters to accuracies on the order of 0.1 mas, and to strengthen the terrestrial reference frame. A catalog based on the radio positions of 560 extragalactic sources distributed over the entire sky was presented by Johnston et al. (1995). The positional accuracy of these sources was estimated to be better than 3 mas in both coordinates, with the majority of the sources having errors better than 1 mas. This catalog marks a milestone in defining a global, self-consistent, inertial radio reference frame accurate on the sub-milliarcsecond level.

Extragalactic radio sources are assumed to be very distant and, thus, they should exhibit little or no detectable proper motion. The reference frame defined by the positions of extragalactic radio sources given by Johnston et al. (1995) can therefore be said to be a quasi-inertial frame (i.e., a frame whose basis is inertial) with little or no time dependency. However, many extragalactic sources have structure on milliarcsecond scales at radio frequencies and temporal variations of the structure will result in apparent motion when astrometric observations are made at several epochs.

If the radio reference frame sources were to display no (real or apparent) proper motion in the future, maintenance of the frame would not be required to keep it at the current level of accuracy. However, some of the sources, notably 0923 + 392 (4C 39.25) and others, have apparent motions in their astrometric positions due to assumed intrinsic structure variations (Eubanks et al. 1996). Thus, the apparent positions of some sources do indeed vary with time. Since even apparently stable sources can suddenly begin exhibiting rapid structure changes (see Wehrle, Cohen, & Unwin 1990), the entire reference frame catalog must be reobserved over time to ensure its continued precision on the sub-milliarcsecond level and to improve it. It is imperative that we understand the impact of radio source structure on the accuracy of individual position determinations as well as on the frame itself.

To this end, we have started an observing program to image the reference frame sources on a regular basis. The goal of these observations is to establish a database of images of all the reference frame sources at the same frequencies as those used for precise astrometry. Most of the reference frame sources have never been imaged, either with sufficient sensitivity, sufficient resolution, or at these frequencies. In addition to providing a larger data set to improve positional accuracy, these observations will allow us primarily to monitor sources for variability or structural changes so they can be evaluated for continued suitability as reference frame objects. Further, these observations will aid in our understanding of the underlying astrophysical phenomena responsible for variations of the intrinsic structure of extragalactic radio sources.

Of the 560 extragalactic sources for which positions were reported by Johnston et al. (1995), a total of 436 sources were used to "define" a radio reference frame. Positions for an additional 124 sources were also presented, in the same frame as that of the defining sources. We report here first-epoch dual-frequency Very Long Baseline Array (VLBA) 2 GHz and 8 GHz observations of a sample of 42 of these 560 sources. The 42 sources presented in this paper were, for the most part, chosen because they were the most troublesome, and hence the most interesting, of the sources in the astrometric analysis. Fourteen of the sources observed here were rejected as defining reference frame objects by Johnston et al. (1995) on the basis of the astrometric analysis. These 14 sources showed inconsistencies in their derived positions when examined on an epoch-by-epoch basis, presumably a direct result of variable intrinsic structure. The remaining 28 sources for which we report observations were either among those used by Johnston et al. (1995) to define the radio frame or were designated as candidate sources possibly to be included in the definition of the frame at a future date. The observations reported here represent the first in a series of observations intended to image the entire set of sources presented by Johnston et al. (1995). Observations from subsequent epochs will be reported as they are reduced and analyzed.

2. OBSERVATIONS AND DATA ANALYSIS

Observations were made during a 24 hr period on 1994 July 8–9 using the Very Long Baseline Array telescope (Napier et al. 1994) of the National Radio Astronomy Observatory (NRAO).[1] Eight IFs (frequency channels) were recorded simultaneously, each 4 MHz wide, with four at S band (centered at 2.22, 2.23, 2.29, and 2.32 GHz) and four at X band (centered at 8.15, 8.23, 8.41, and 8.55 GHz) for a total bandwidth of 16 MHz in each frequency band. Observations were made in a dual-frequency bandwidth synthesis mode to facilitate delay measurements for astrometry. The multiplicity of channels allows for the determination of a precise group delay (Rogers 1970), while simultaneous observations in two bands allows for an accurate calibration of the frequency-dependent propagation delay introduced by the ionosphere. Results of the precise astrometry afforded by these observations will be presented elsewhere. Observations in this mode also allow simultaneous dual-frequency imaging, which is the focus of the work discussed here.

Forty-two sources were observed using short-duration ($\sim$4 minute) "snapshots" over a number of different hour angles to maximize the (u, v) coverage. Observations were scheduled to maximize mutual visibility between the VLBA antennas, so low-declination sources were usually observed less often than those at higher declinations. Most sources were observed during at least five or six scans, while a few sources were observed during as many as 12 scans. No source was observed during fewer than four scans. Sample plots of the combined (u, v) coverage from the four S-band IFs (2.22–2.32 GHz) for sources at different declinations are shown in Figure 1. The combined (u, v) coverage from the four X-band IFs (8.15–8.55 GHz) is identical to that at S band, except for a scaling factor equal to the ratio of the observing frequencies.

The raw data bits were correlated with the VLBA correlator at the Array Operations Center in Socorro, New Mexico. The correlated data were calibrated and corrected for residual delay and rate using the NRAO Astronomical Image Processing System (AIPS). Initial amplitude calibration for each of the eight IFs was accomplished using system temperature measurements taken during the observations and the NRAO supplied gain curves. Fringe-fitting was done in AIPS using solution intervals of 1 minute and a point-source model in all cases. After correction for residual delay and rate, the data were written to FITS disk files. All subsequent processing was carried out using the Caltech VLBI imaging software, primarily DIFMAP. After phase self-calibration with a point source model, the 2 s correlator records were coherently averaged to 10 s records and then edited.

[1] The National Radio Astronomy Observatory (NRAO) is operated by Associated Universities, Inc., under cooperative agreement with the National Science Foundation.

Amplitude calibration was improved by observations of the compact source 1741−038. A single amplitude gain correction factor for 1741−038 was derived for each antenna for each IF, based on fitting a simple Gaussian source model to the 1741−038 visibility data after applying only the initial calibration based on the measured system temperatures and gain curves. Gain correction factors were calculated based on the differences between the observed and model visibilities. A circular Gaussian model with amplitude of 2.1 Jy and FWHM of 0.4 mas was used at S band. The circular Gaussian model used at X band had an amplitude of 3.0 Jy and FWHM of 0.3 mas. The resulting set of amplitude gain correction factors was then applied to the visibility data of 1741−038 as well as to the visibility data of the remaining sources. Evaluation of amplitude ratios at crossing points in the (u, v) plane on a sample of sources confirmed that the relative amplitude calibration at this stage was better than 5% for most antennas but in no case exceeded 10%.

The 1741−038 models at each frequency were found to be consistent with the closure amplitudes. The flux densities were $\sim$10% higher than those measured by the NRAO Green Bank Interferometer (GBI) at the same frequencies (E. Waltman 1995, private communication) averaged over the 2 month period between 1994 April 19 and 1994 June 15. The GBI did not observe 1741−038 after 1994 June 15, so no GBI flux density data were available for the epoch of the VLBA observations. The visibility data were not corrected for this amplitude discrepancy. An additional check on the flux density calibration was performed using the source 1749+096. Model flux densities for 1749+096 were found to be $\sim$20% higher than those measured by the GBI at the same frequencies (E. Waltman 1995, private communication) averaged over an approximately 15 day period centered on the VLBA observations. These results suggest that the absolute flux density calibration is probably good to within about 20%. However, it should be noted that 1741−038 and 1749+096 are known to be highly variable at these frequencies (see Fiedler et al. 1994; Clegg, Fey, & Fiedler 1996).

The visibility data for each frequency band were self-calibrated, Fourier inverted, and CLEANed using DIFMAP in an automatic mode (Shepherd, Pearson, & Taylor 1995). DIFMAP combines the visibilities for each IF of an observation in the (u, v) plane during gridding, taking into account frequency differences. However, DIFMAP makes no attempt to correct for spectral index effects. The spanned bandwidth of the four IFs in each band are relatively small (0.1 GHz [4% fractional bandwidth] at S band and 0.4 GHz [5% fractional bandwidth] at X band), so we assume that source structure and flux density variations across each of the two frequency bands are negligible. The data were self-calibrated following the hybrid-mapping technique (Pearson & Readhead 1984) to correct for residual amplitude and phase errors. The data were initially phase self-calibrated and mapped using uniform weighting in the (u, v) plane before switching to natural weighting after several iterations. A point-source model was used as a starting model for the iterative procedure in all cases. Convergence was usually obtained in 15–20 iterations (including both phase only and phase plus amplitude self-calibration) but went as high as 50 iterations for some of the more extended sources at S band. Convergence was defined basically as the iteration at which the peak in the residual

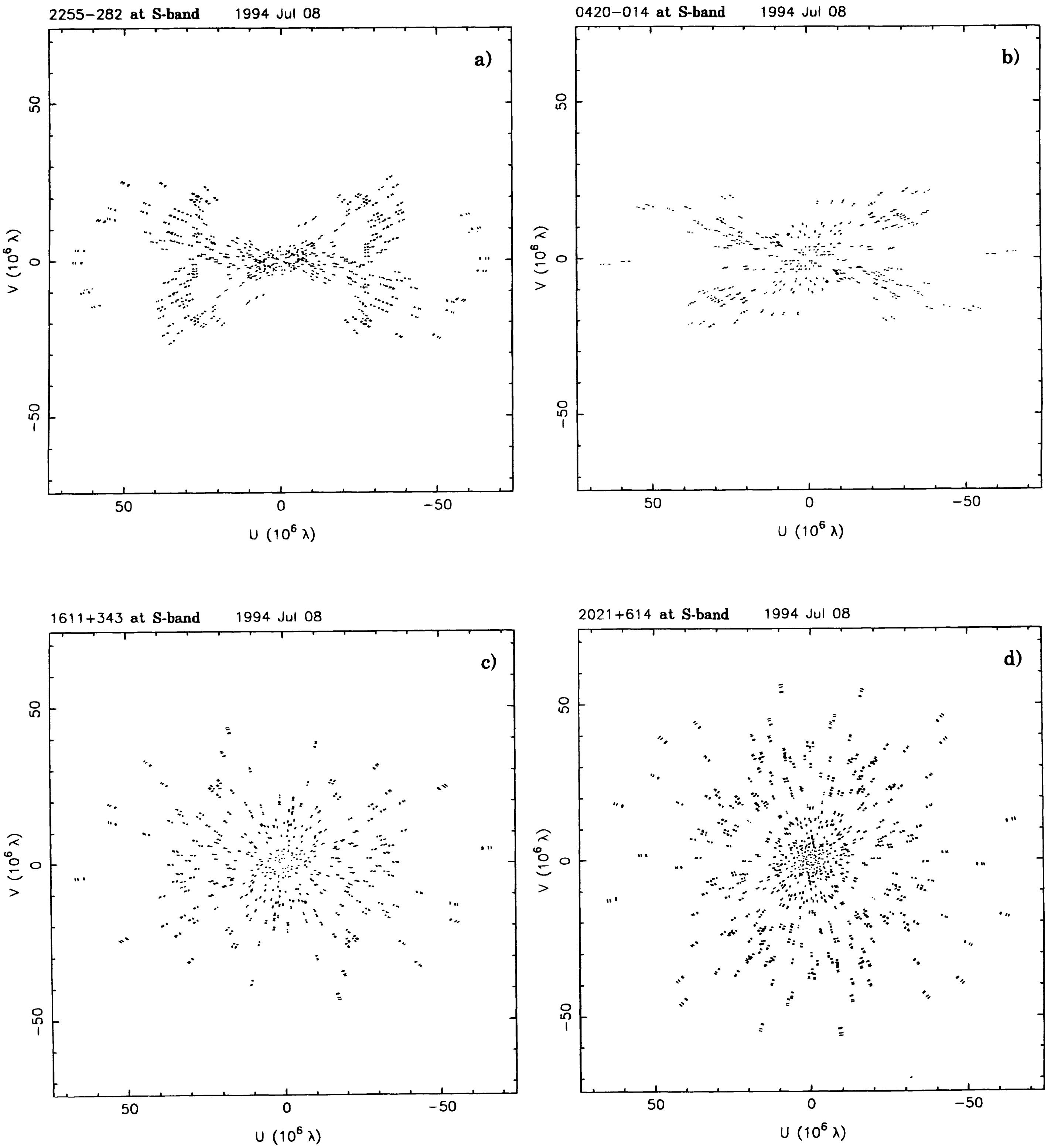

FIG. 1.—Plots of the combined (u, v) coverage from the four S-band IFs (2.22–2.32 GHz) for a sample of sources observed during different numbers of scans and with different declinations. The declination and the number n of approximately 4 minute scans represented in each panel are (a) $\delta \approx -30°$, $n = 5$; (b) $\delta \approx 0°$, $n = 4$; (c) $\delta \approx 35°$, $n = 5$; and (d) $\delta \approx 60°$, $n = 9$. The combined (u, v) coverage at X band (8.15–8.55 GHz) is identical to that at S band, except for a scaling factor equal to the ratio of the observing frequencies.

image became less than a specified factor times the root mean square (rms) noise of the residual image from the previous iteration.

3. RESULTS

For convenience, the resulting images for each band will be referred to by only a single fiducial frequency (2.32 GHz and 8.55 GHz, respectively), even though they were made using the data from all frequency channels. Contour plots of the final naturally weighted images of 42 sources at both 2.32 GHz and 8.55 GHz are shown in Figure 2. Table 1 lists parameters of the final images. The maximum dynamic

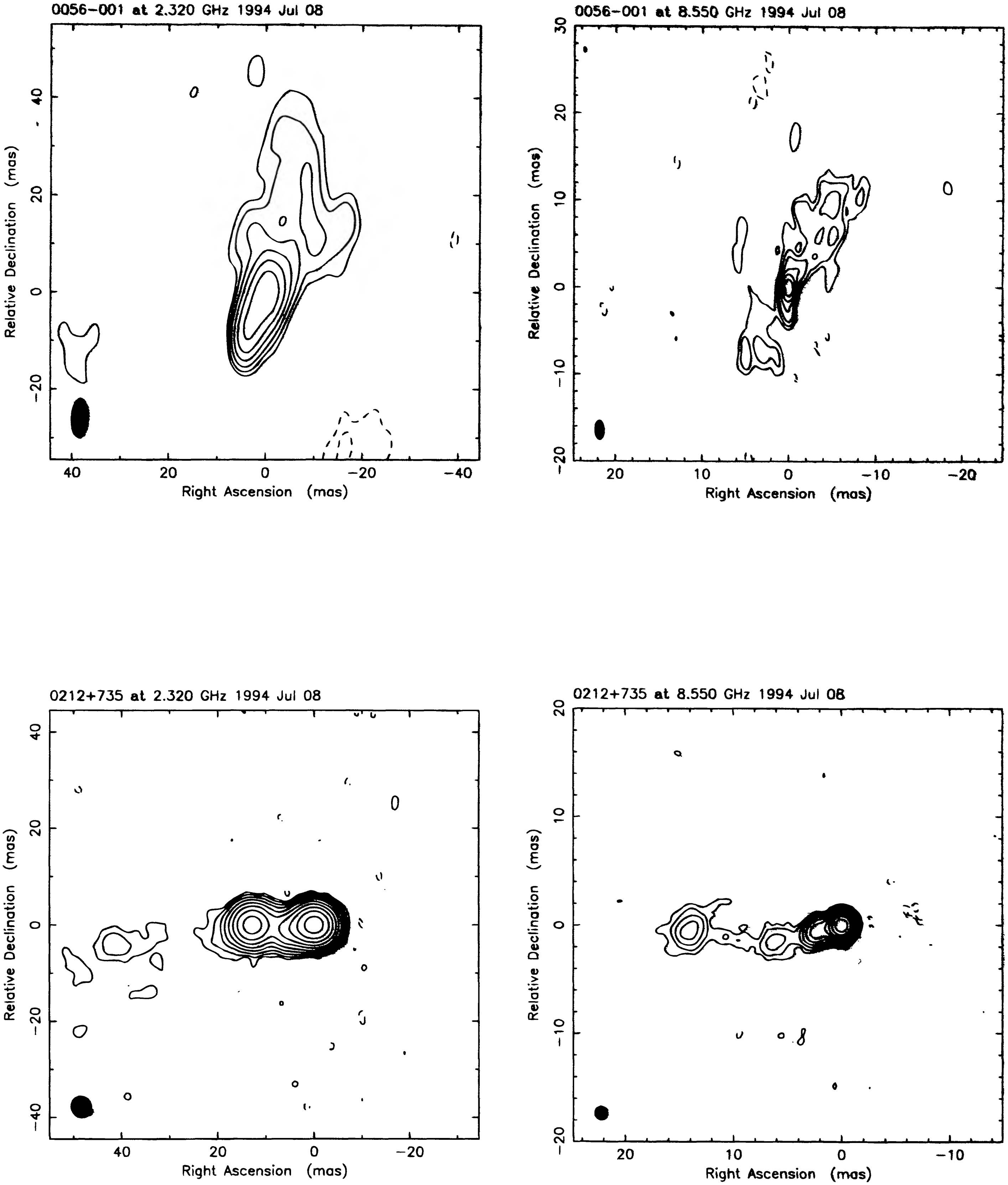

FIG. 2.—Contour plots of 42 radio reference frame sources at both 2.32 GHz and 8.55 GHz. Image parameters are listed in Table 1. Gaussian models fitted to the visibility data at each frequency are listed in Table 2. The FWHM restoring beam applied to the images is shown as a hatched ellipse in the lower left of each panel. For convenience, the images for each band are labeled only by a single fiducial frequency (2.32 GHz and 8.55 GHz, respectively) even though they were made using the data from all frequency channels (see text). Milliarcsecond accurate positions for these sources can be obtained from Johnston et al. (1995).

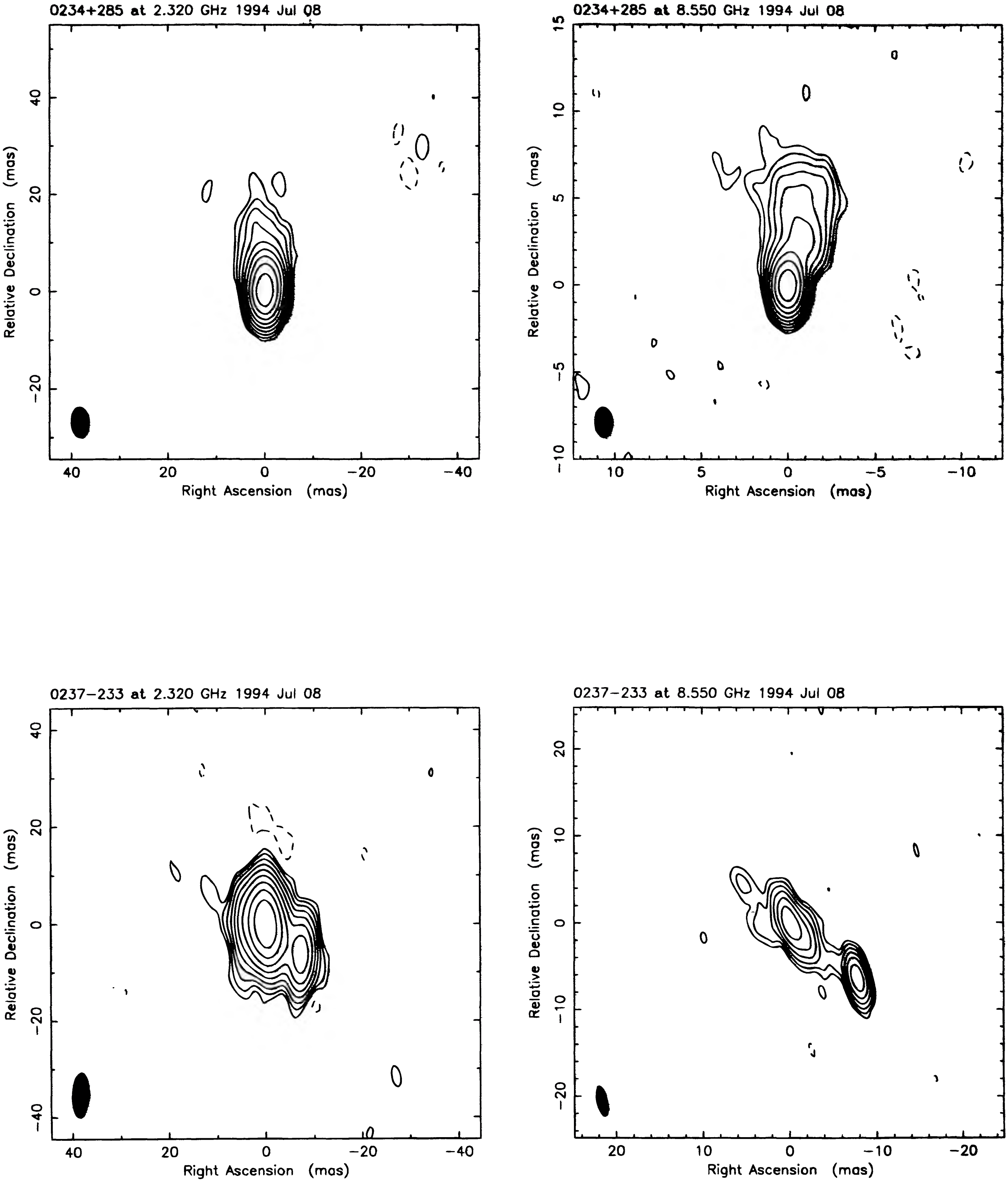

FIG. 2—*Continued*

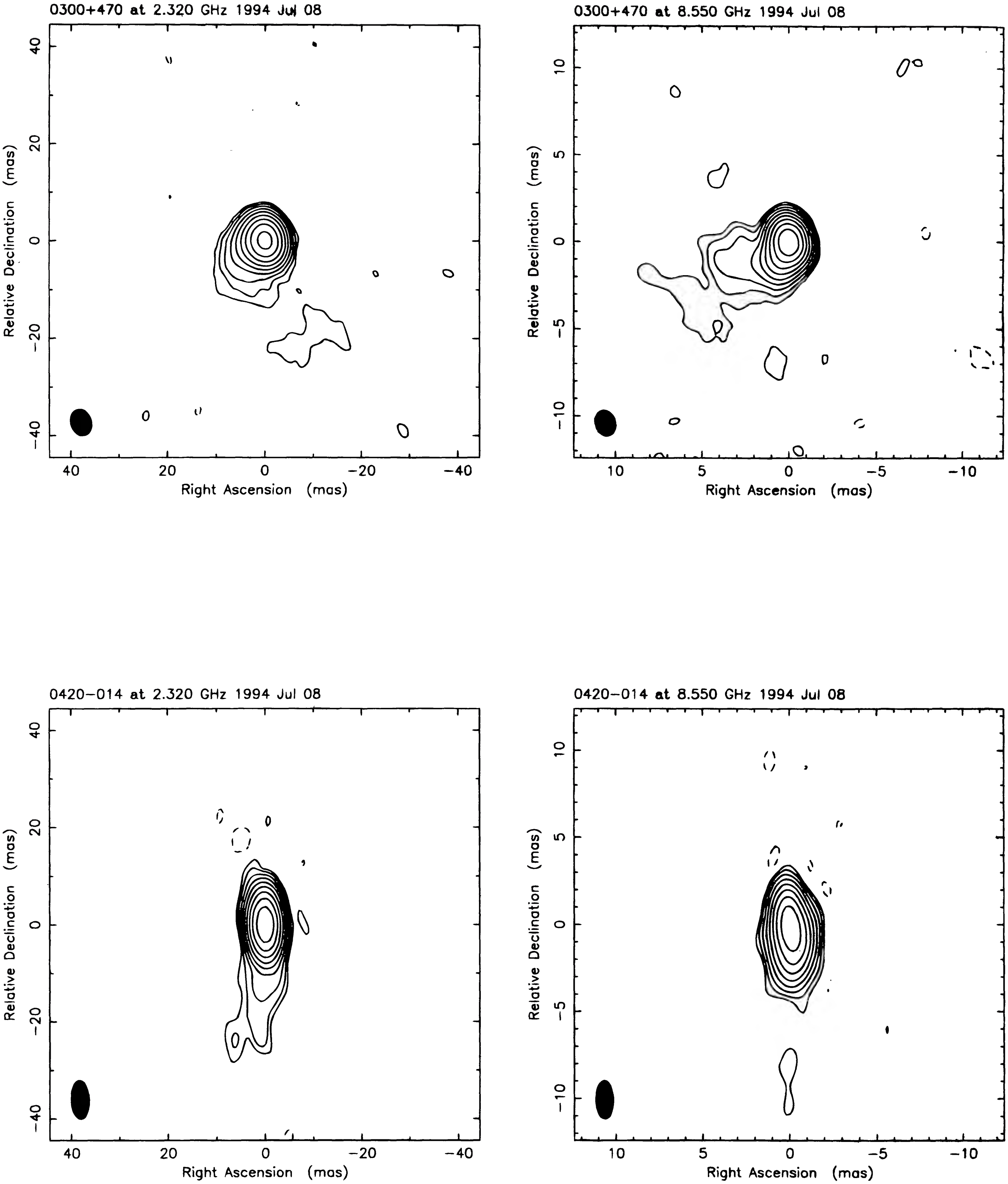

FIG. 2—*Continued*

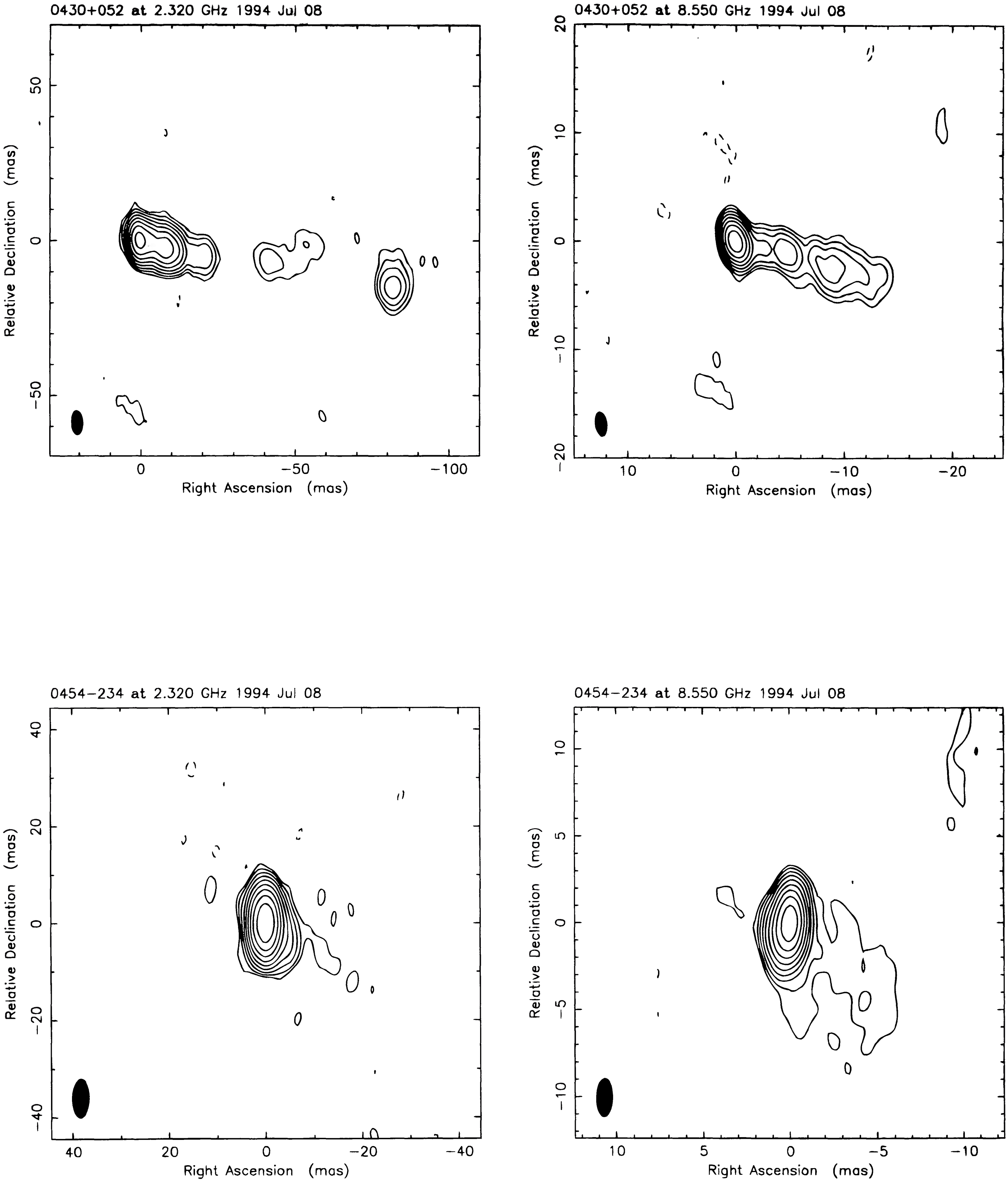

FIG. 2—*Continued*

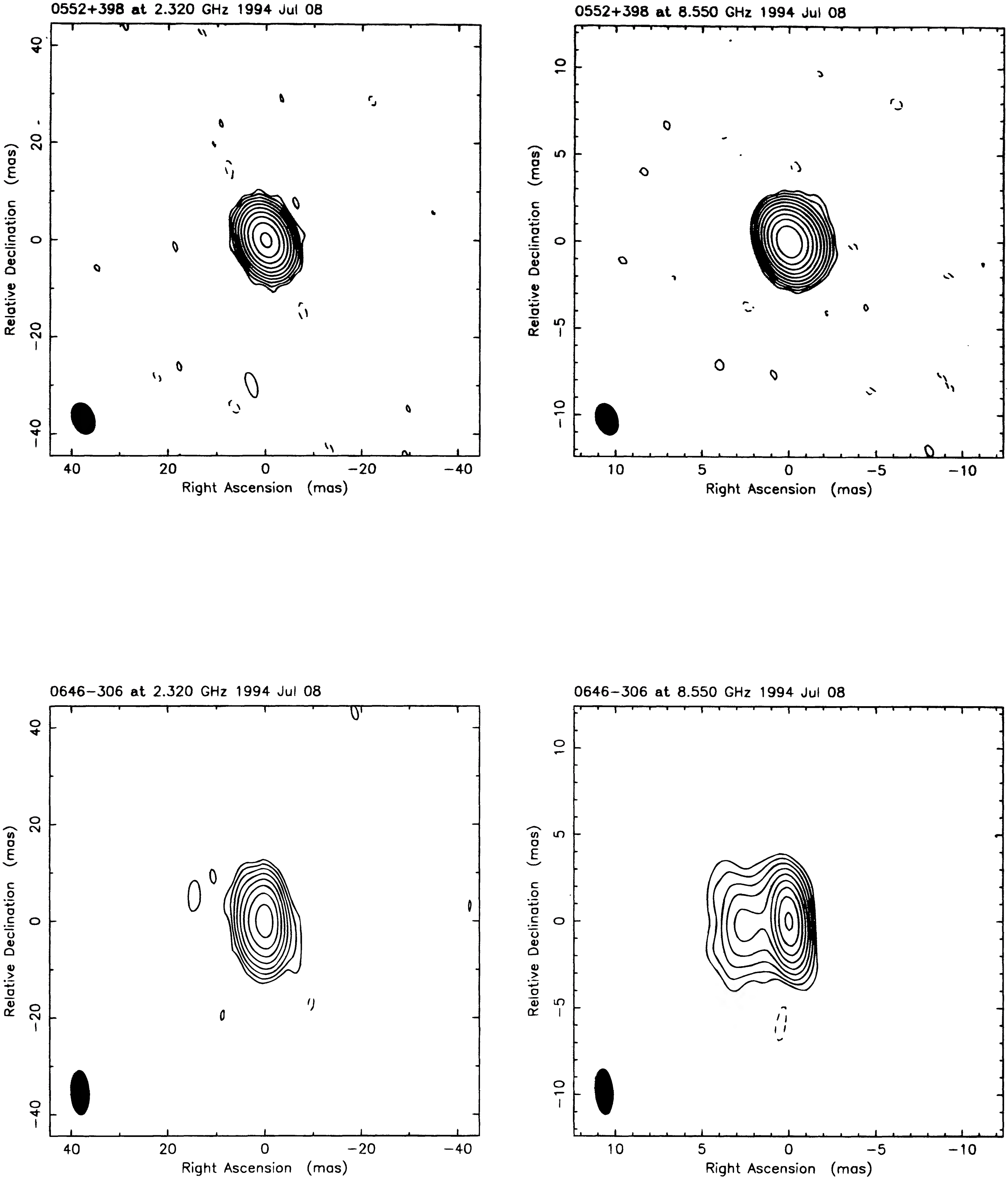

FIG. 2—*Continued*

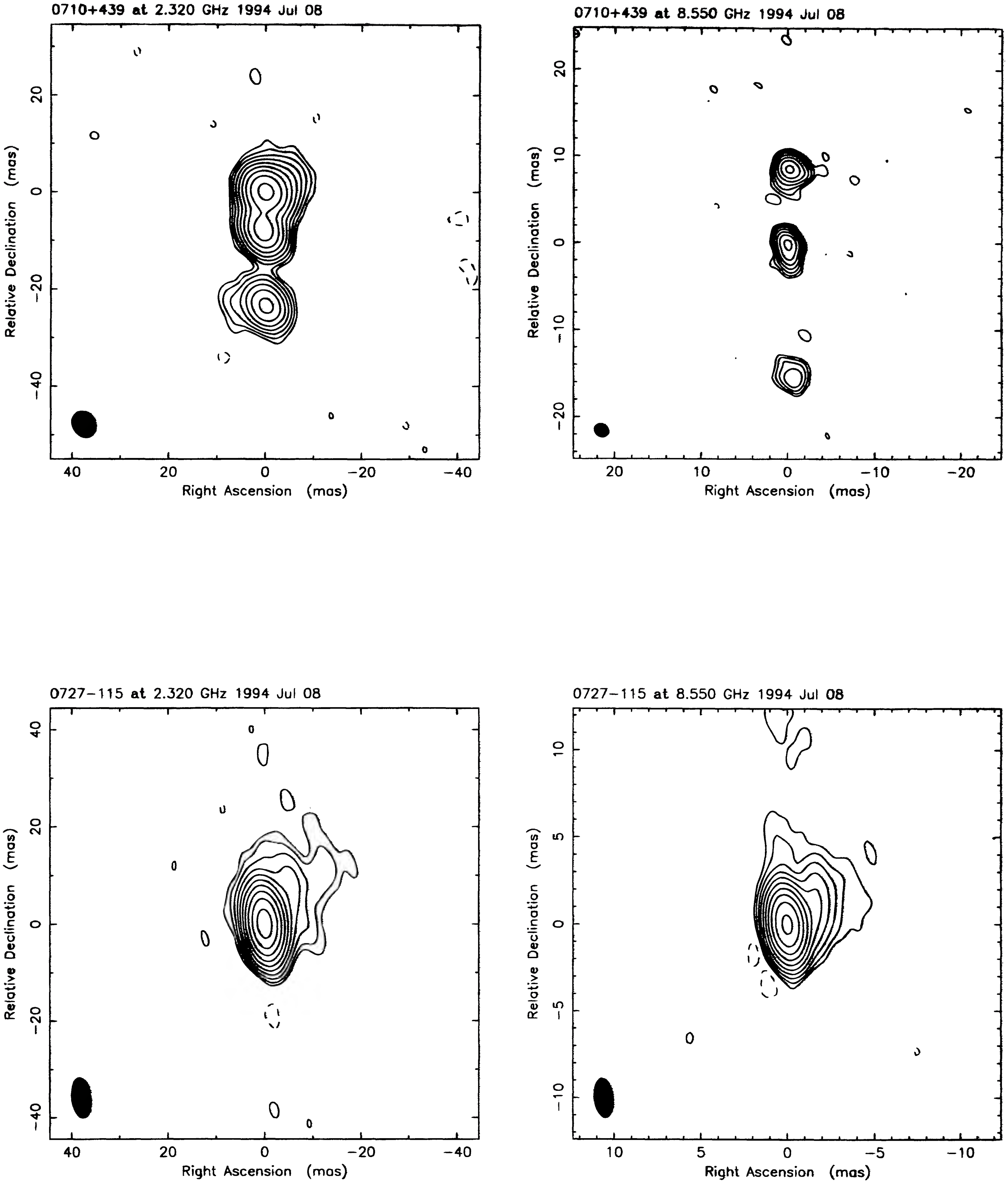

FIG. 2—*Continued*

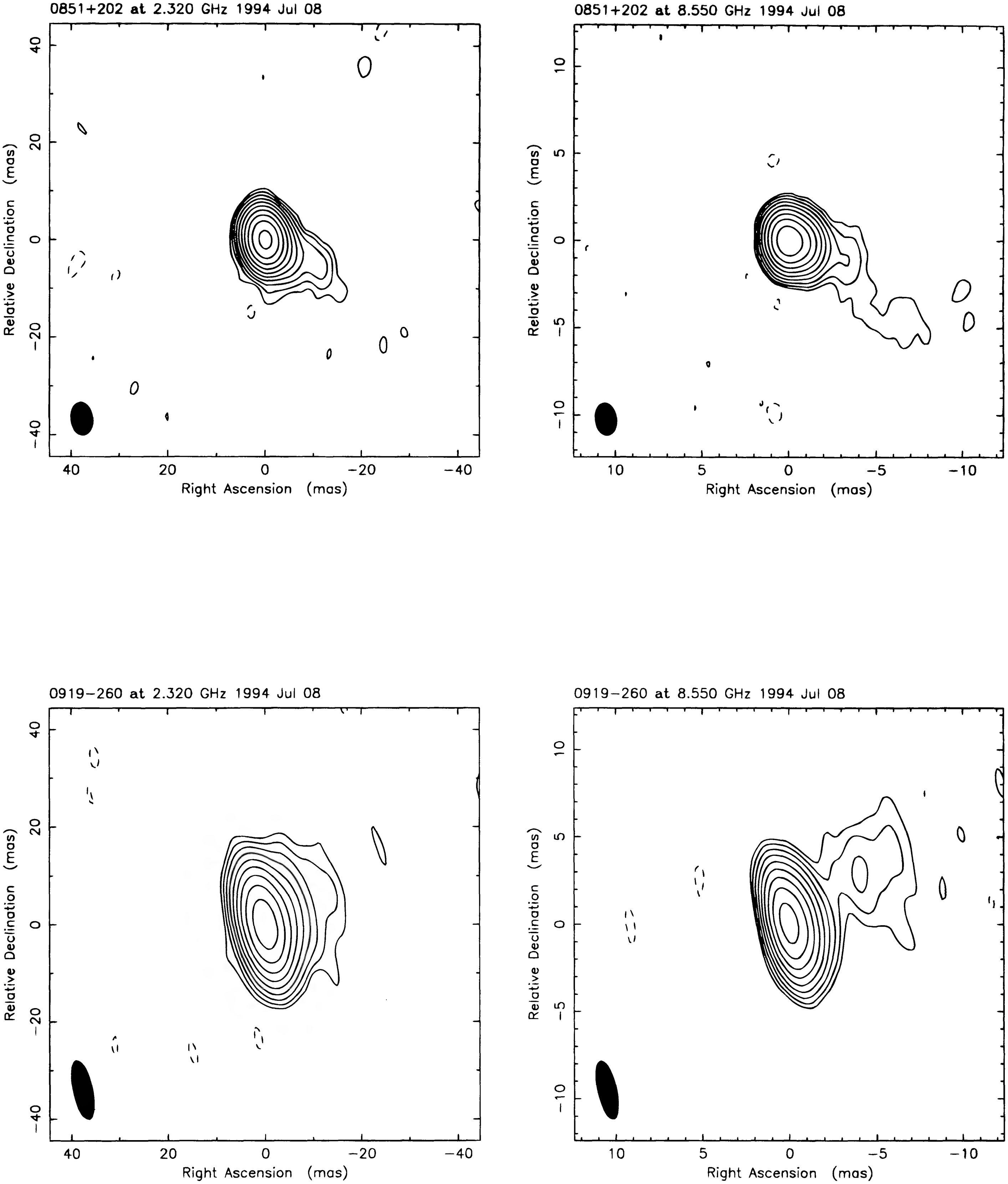

FIG. 2—*Continued*

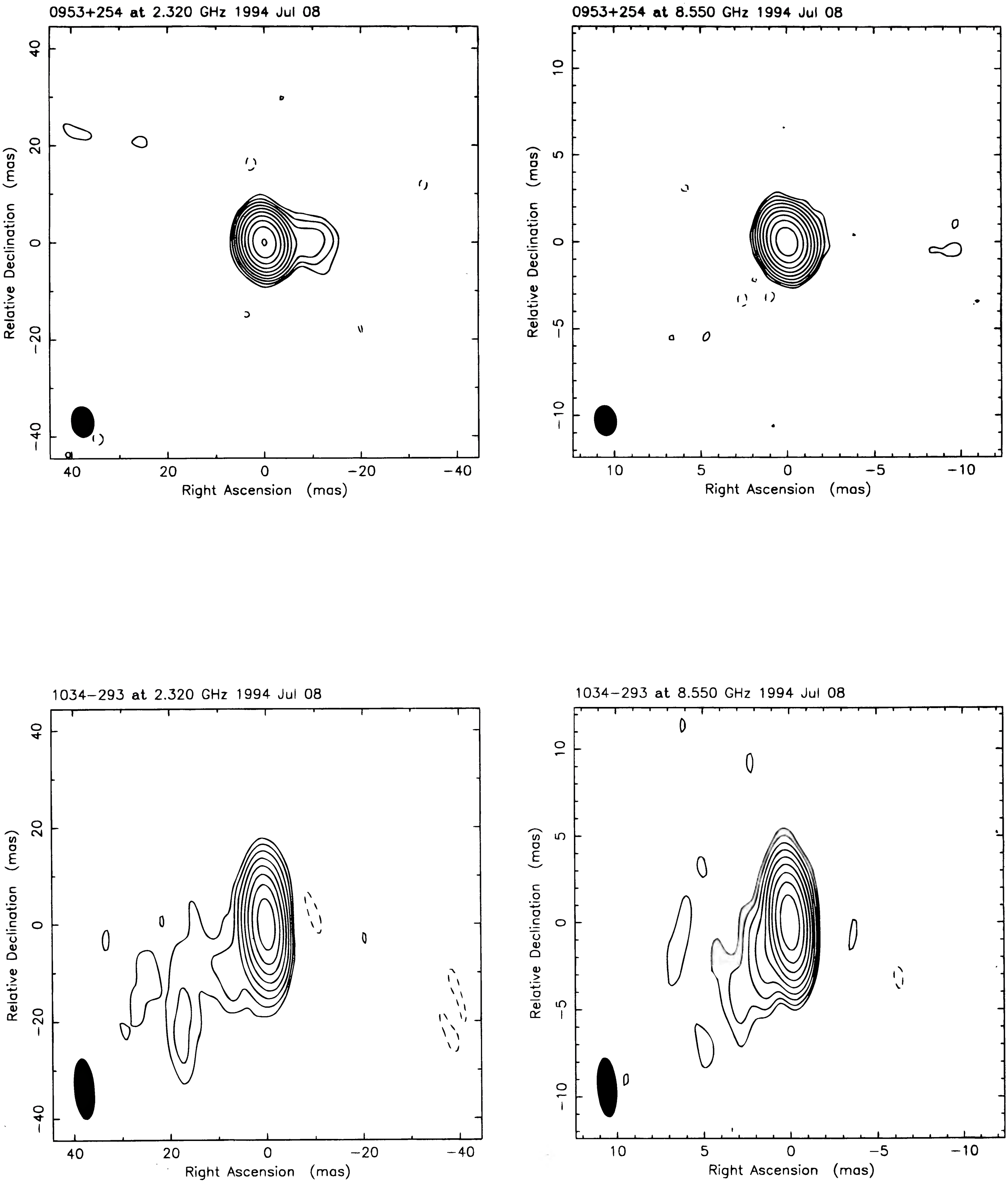

FIG. 2—*Continued*

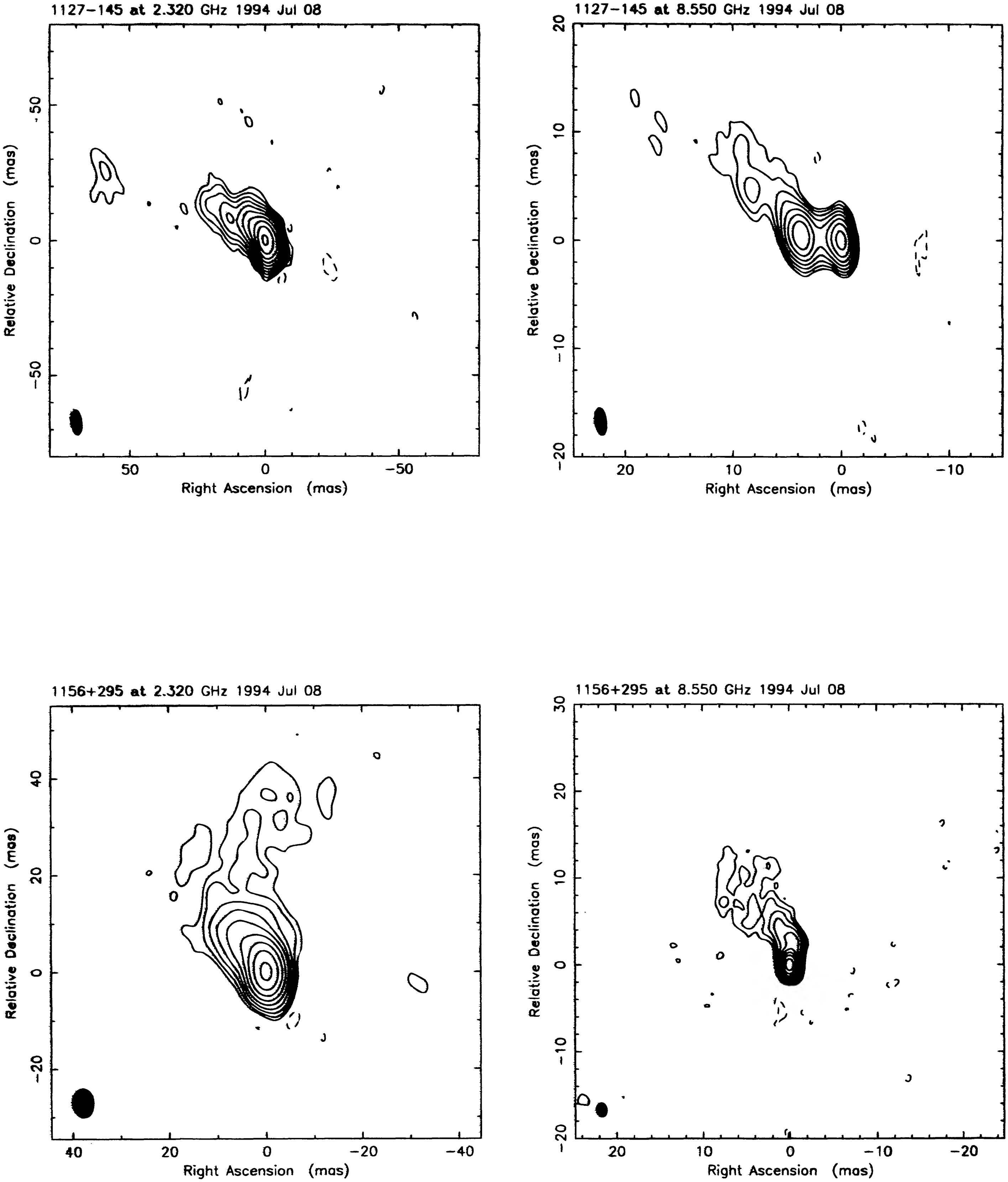

FIG. 2—*Continued*

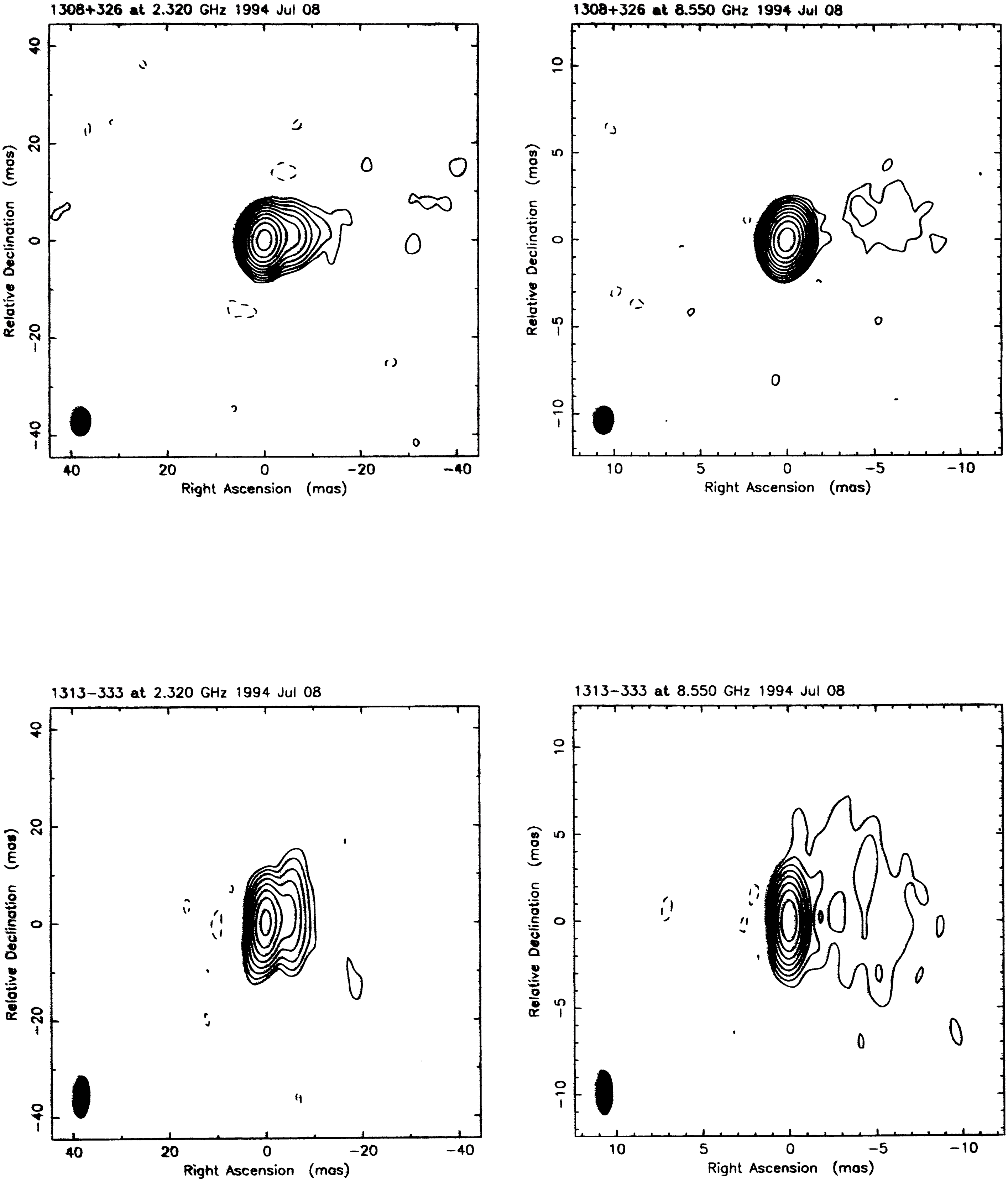

FIG. 2—*Continued*

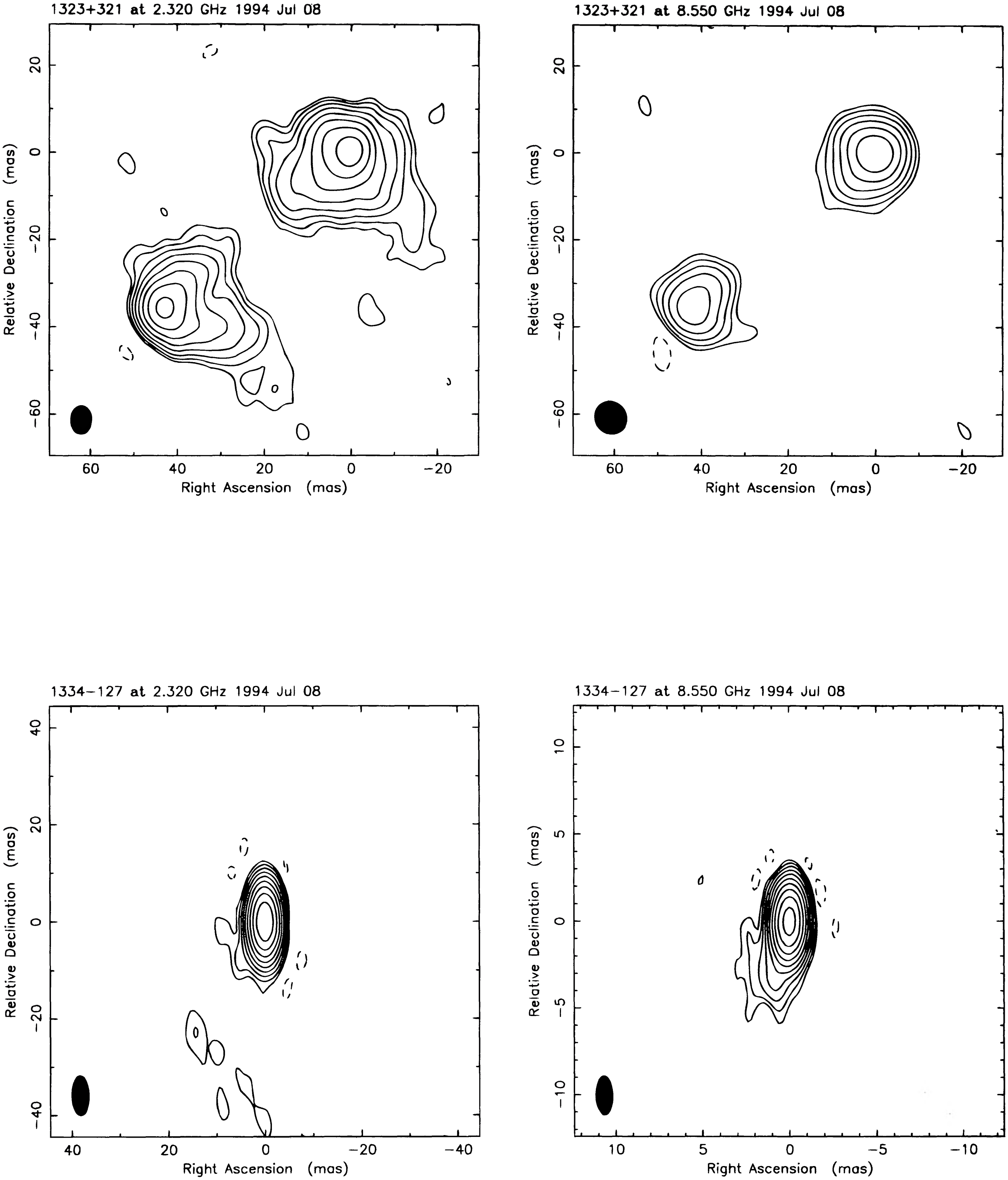

FIG. 2—*Continued*

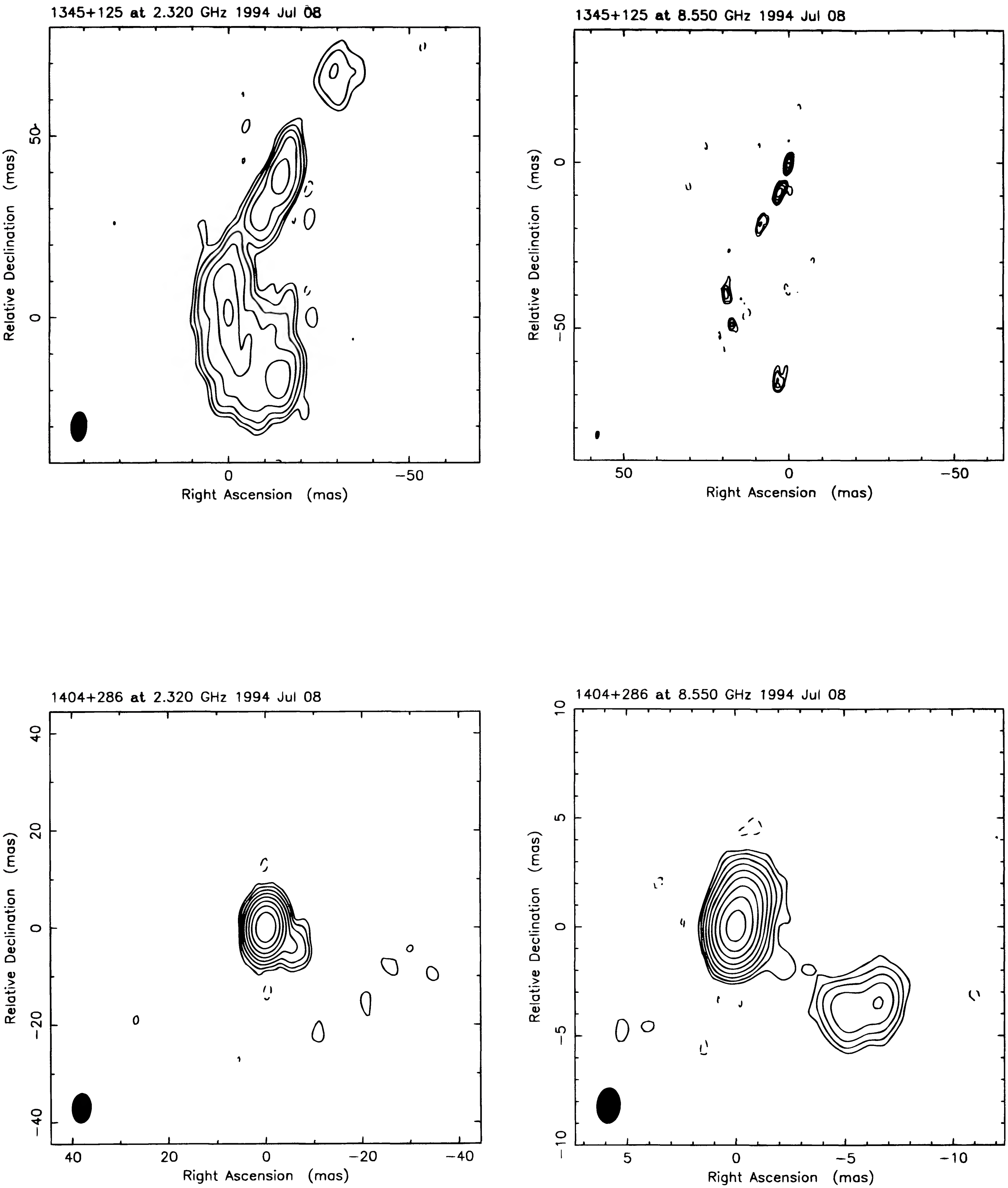

FIG. 2—*Continued*

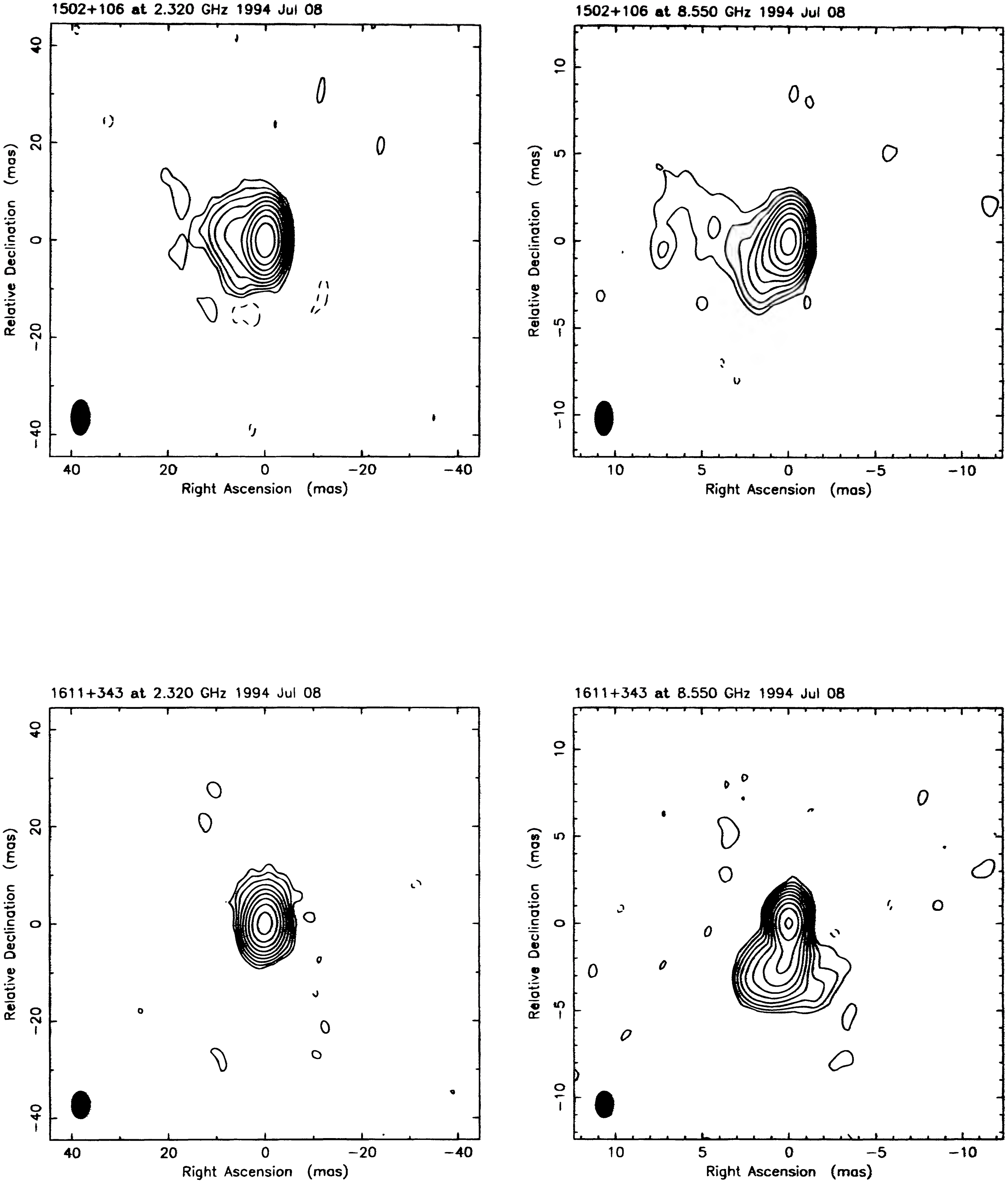

FIG. 2—*Continued*

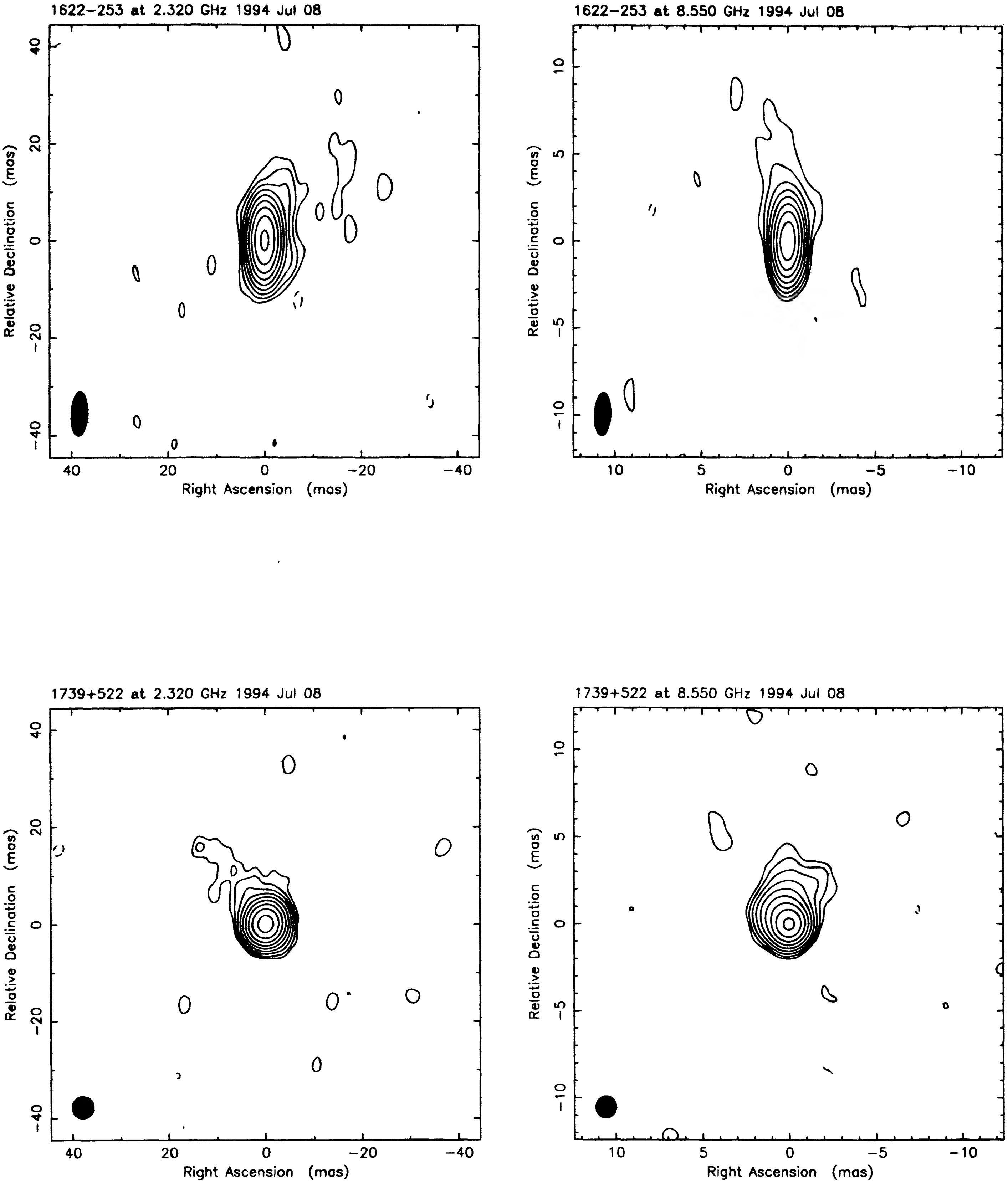

FIG. 2—*Continued*

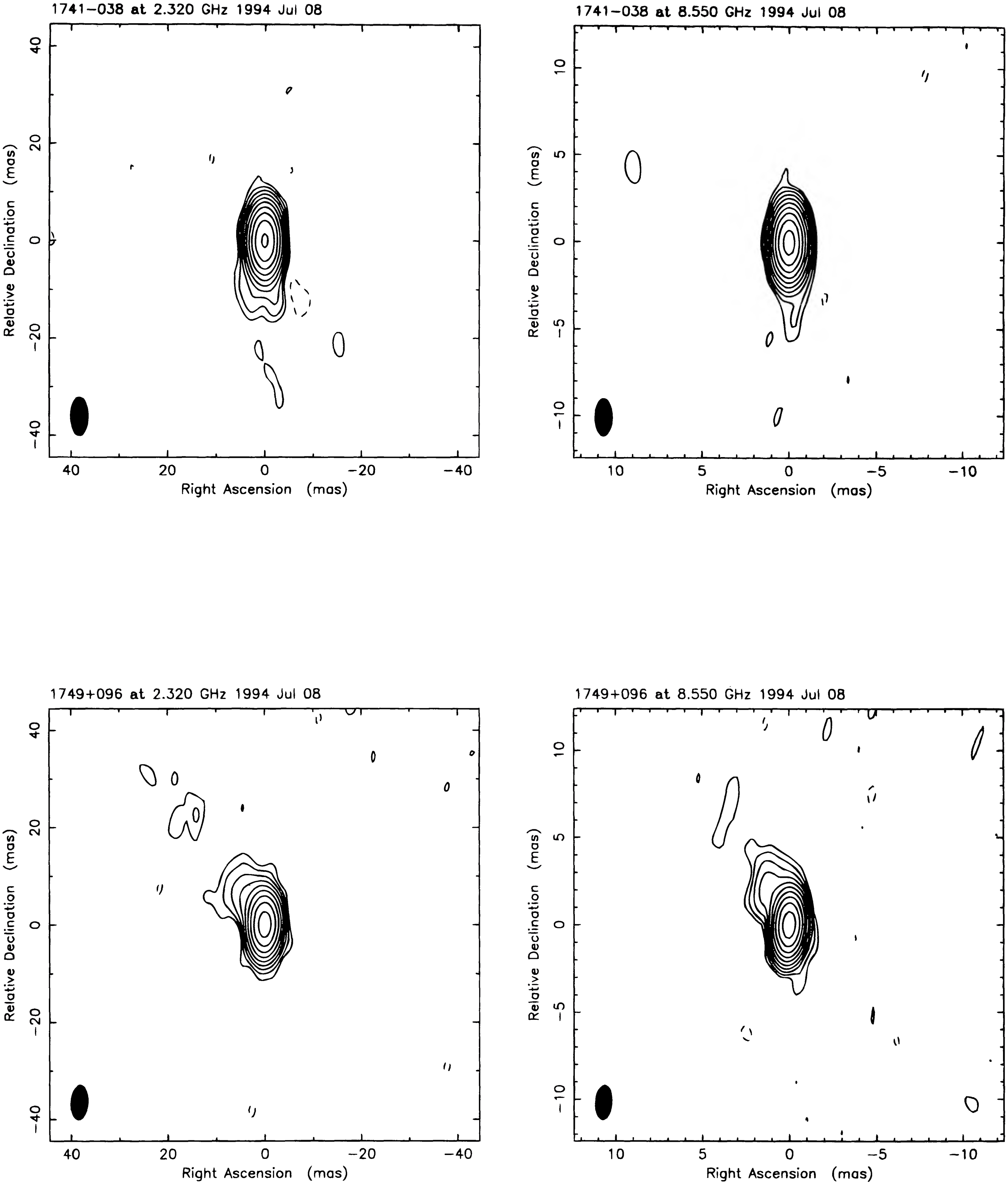

FIG. 2—*Continued*

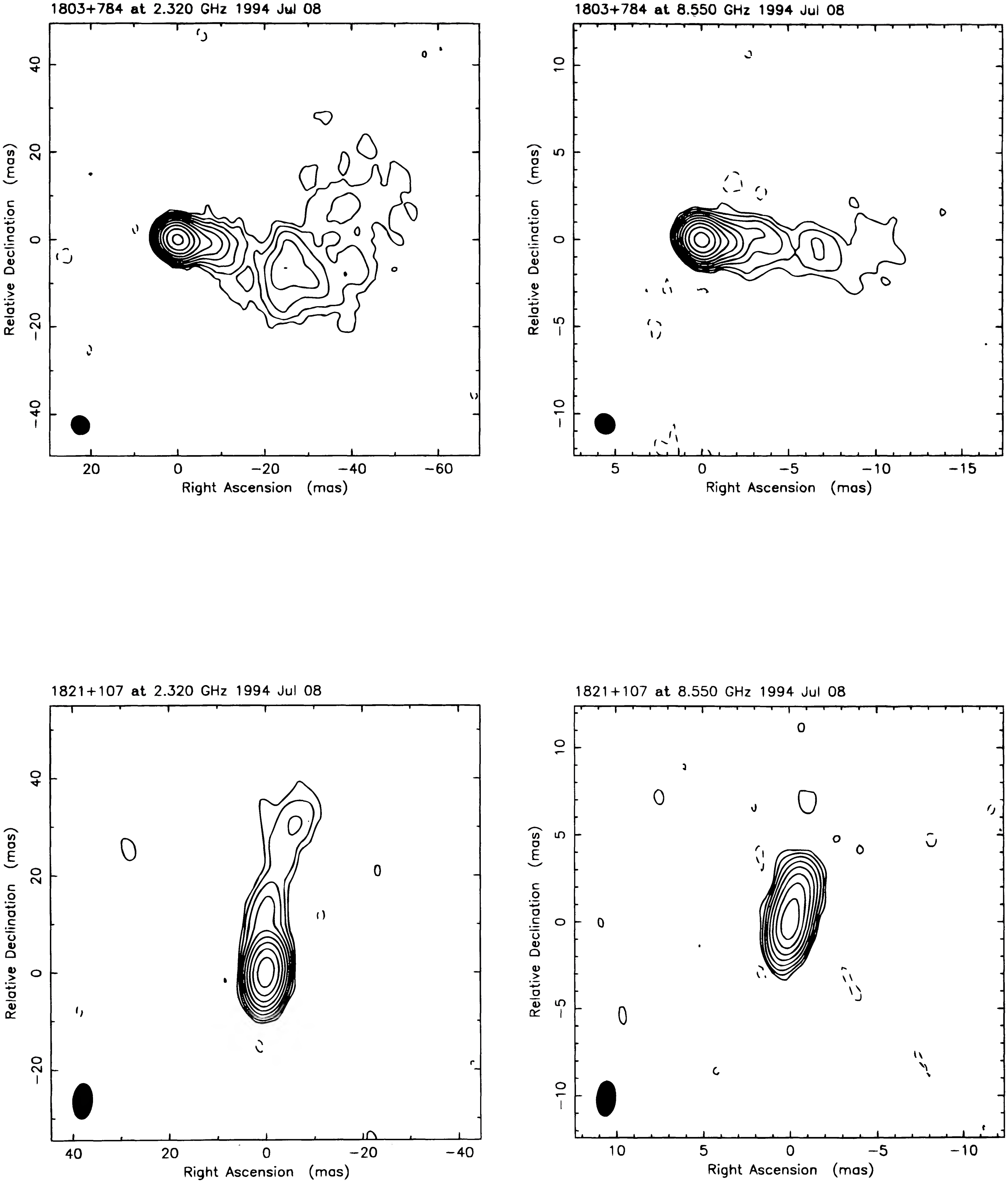

FIG. 2—*Continued*

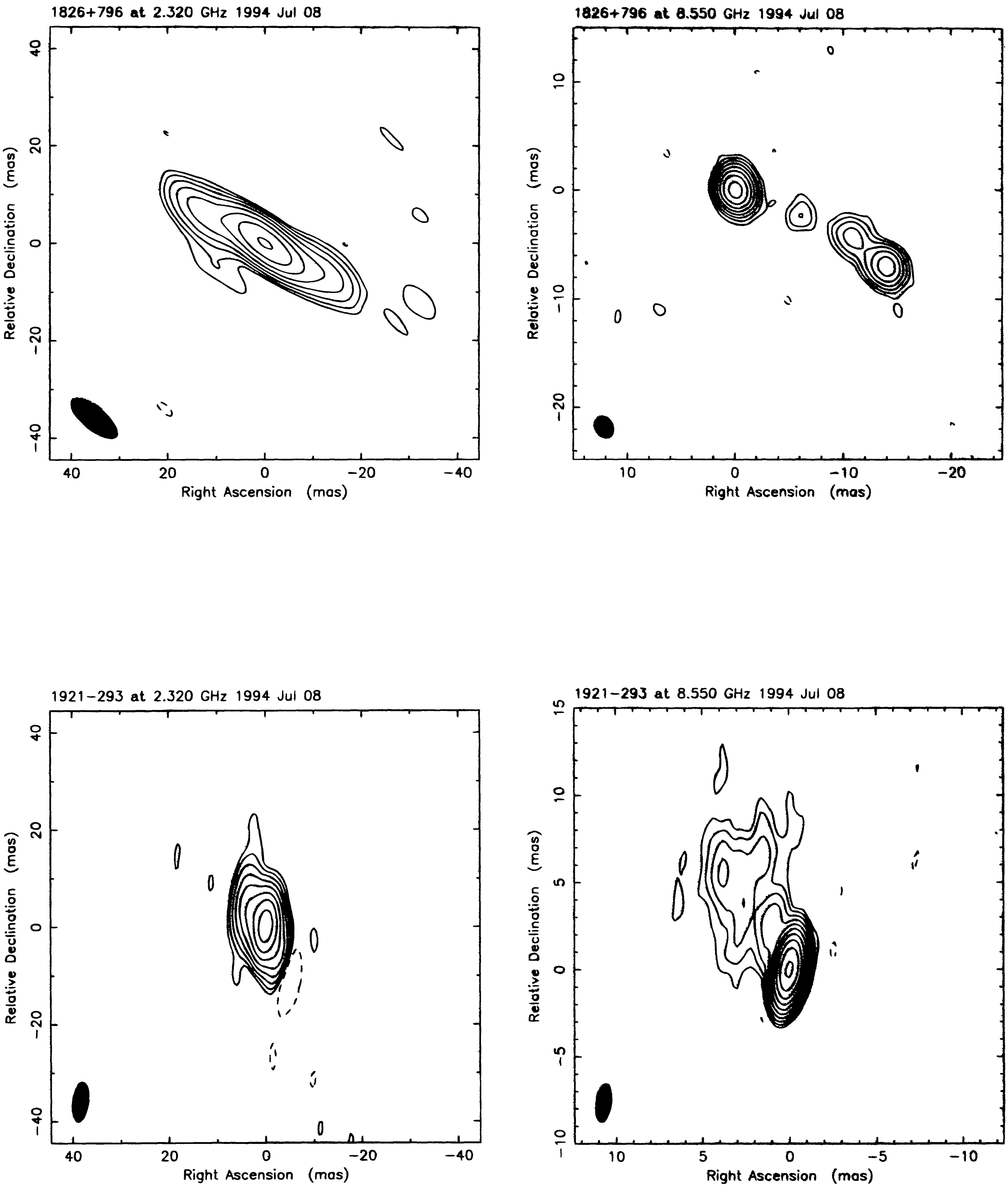

FIG. 2—*Continued*

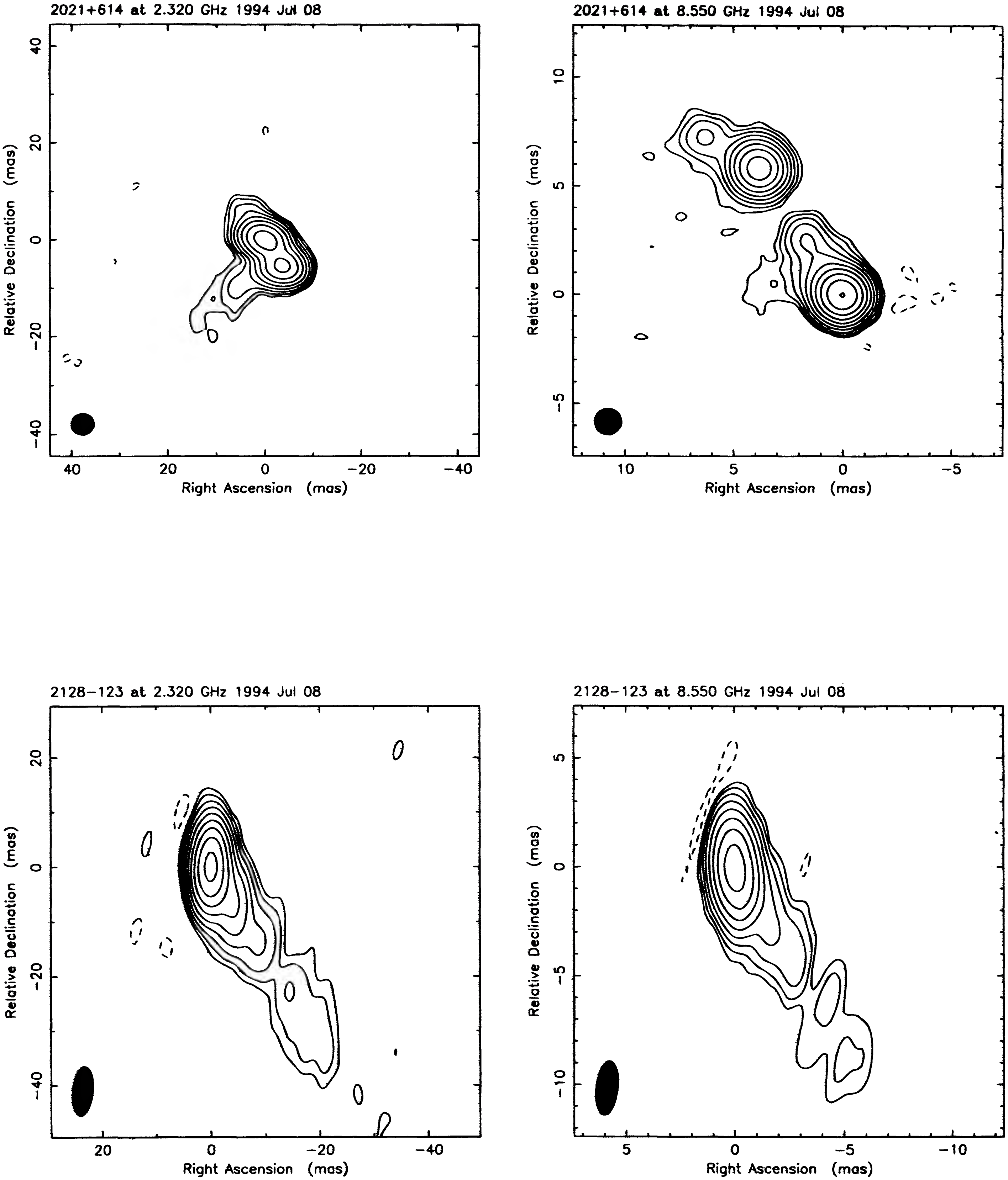

FIG. 2—*Continued*

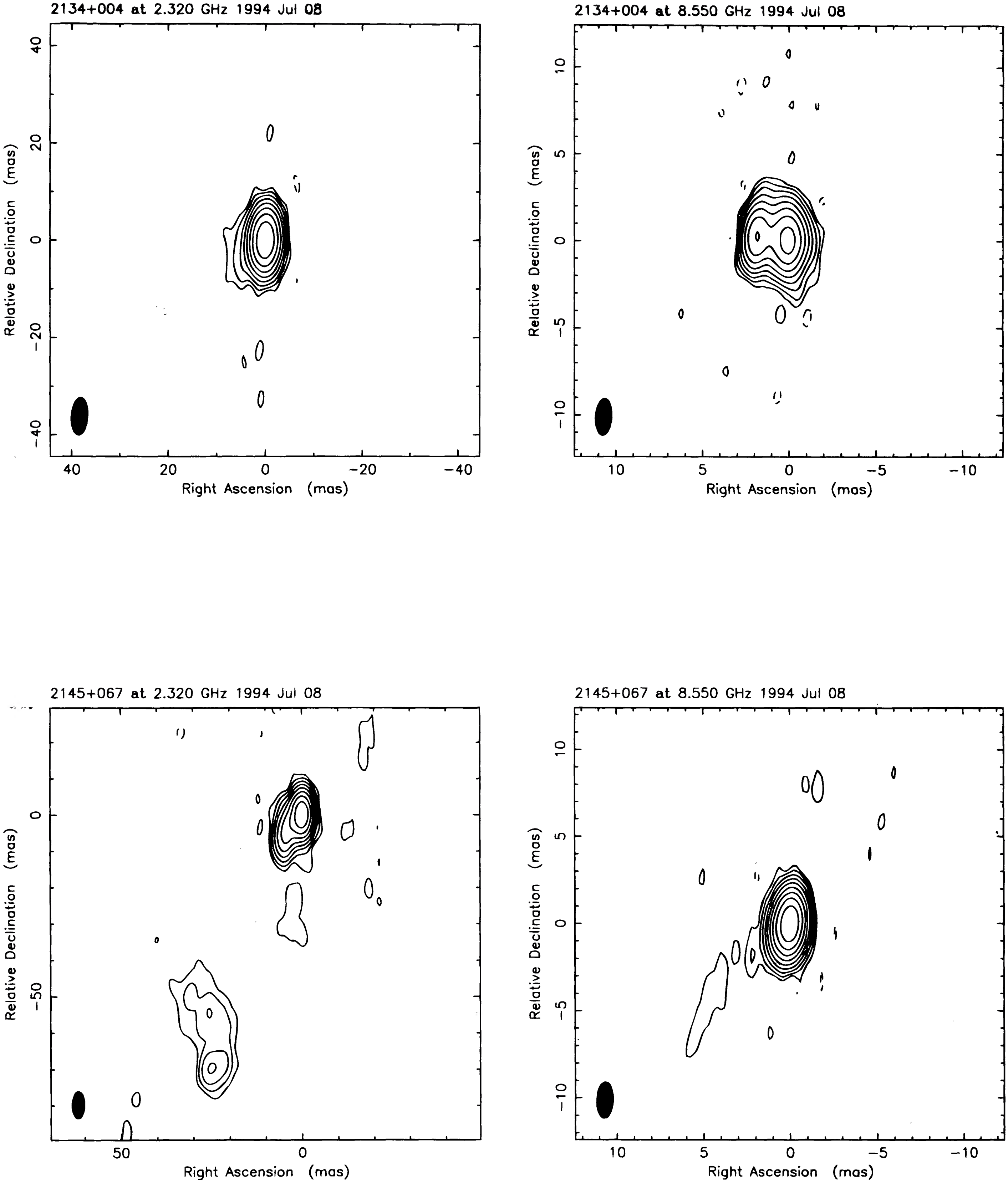

FIG. 2—*Continued*

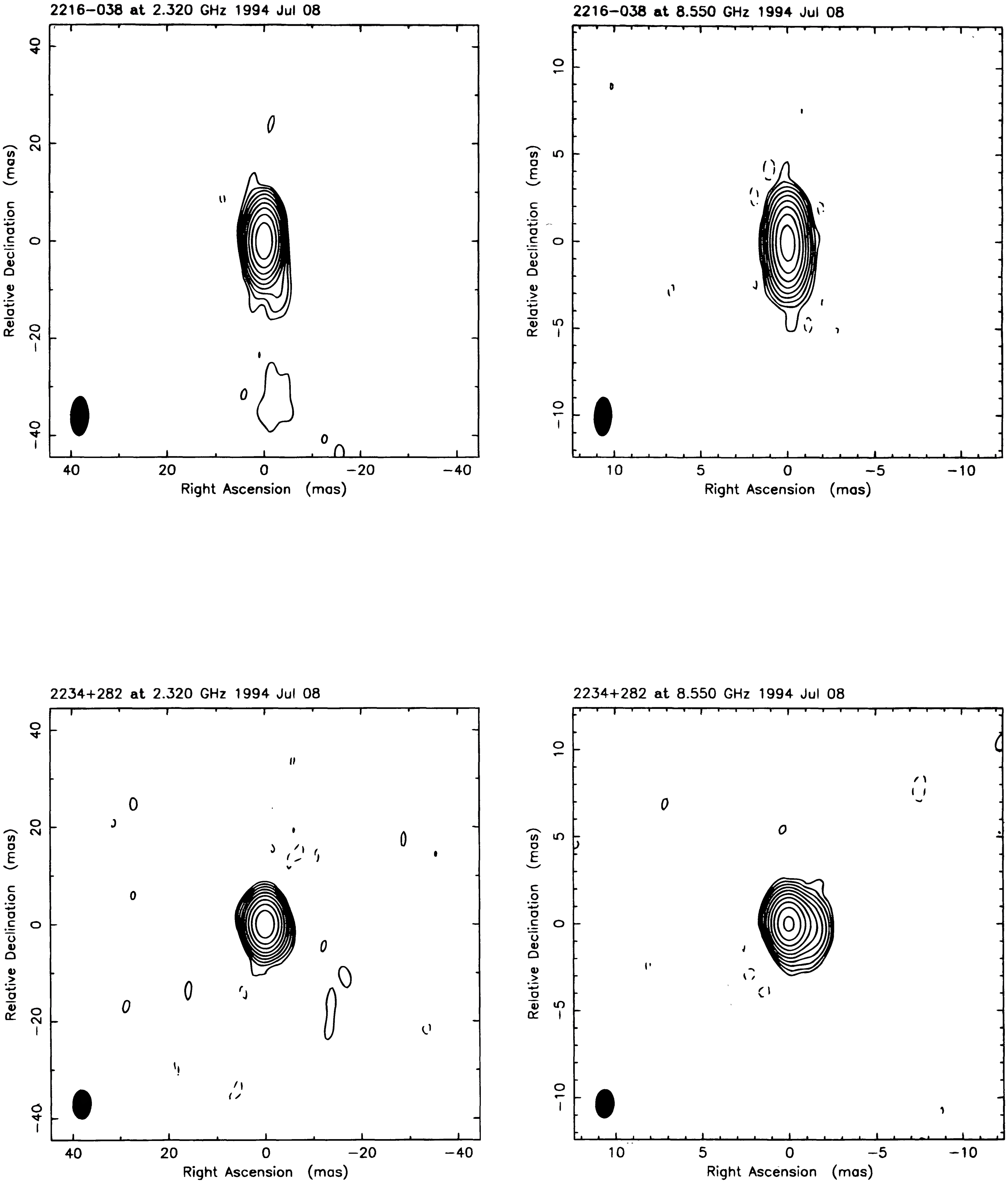

FIG. 2—*Continued*

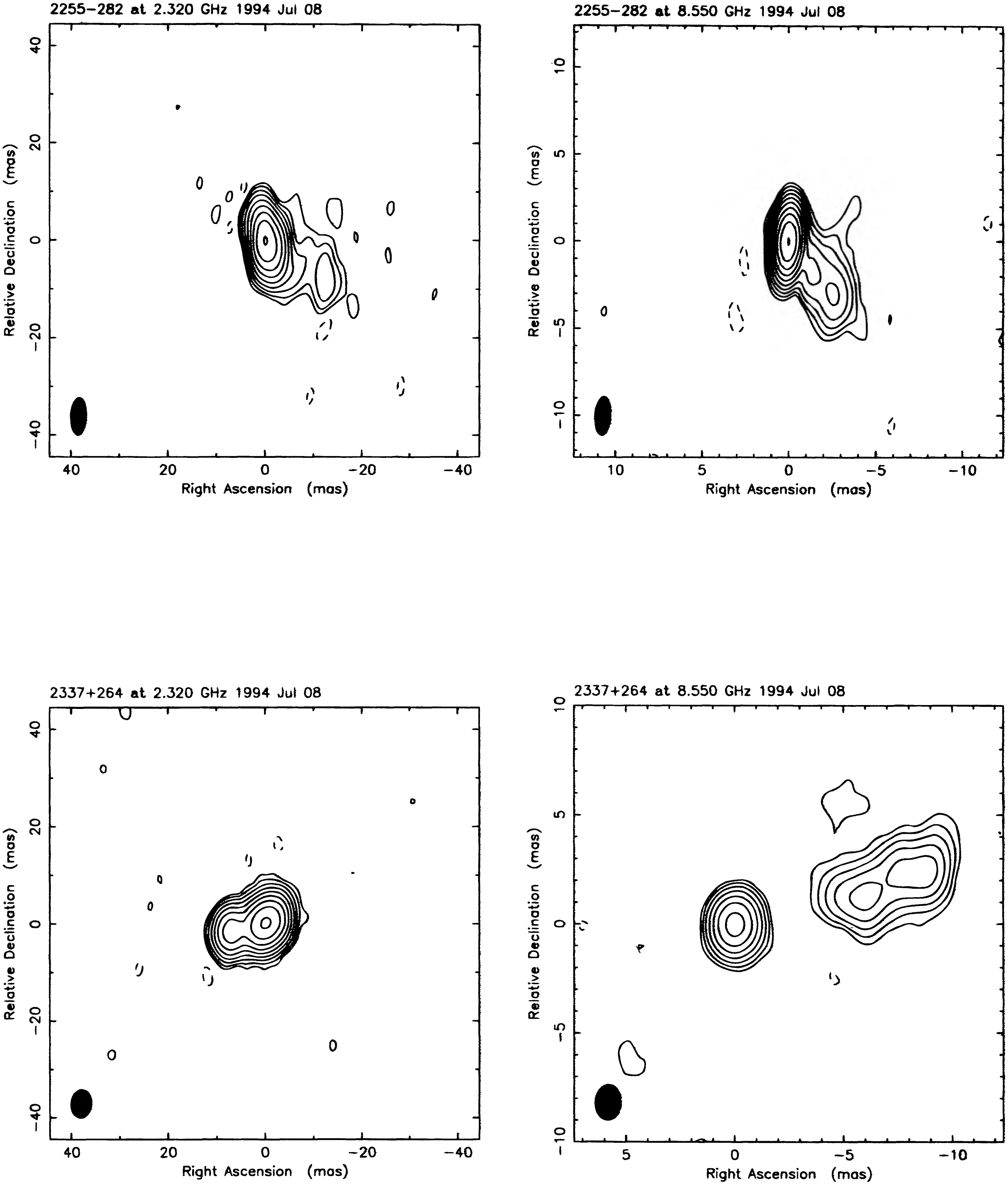

FIG. 2—*Continued*

TABLE 1

Parameters of Naturally Weighted Images

Source	ν (GHz)	Beam[a] a (mas)	Beam[a] b (mas)	Beam[a] ϕ	Peak (Jy beam^{-1})	rms[b] (mJy beam^{-1})	Contour Levels[c] (mJy beam^{-1})
0056−001......	2.32	8.1	3.5	−2°	0.52	2.7	$8.2 \times (1, \ldots, 2^5)$
	8.55	2.1	1.0	2	0.16	1.0	$3.1 \times (1, \ldots, 2^5)$
0212+735......	2.32	4.6	4.2	30	1.81	0.8	$2.3 \times (1, \ldots, 2^9)$
	8.55	1.3	1.2	22	2.65	0.8	$2.9 \times (1, \ldots, 2^9)$
0234+285......	2.32	6.3	3.7	5	2.20	1.3	$5.1 \times (1, \ldots, 2^8)$
	8.55	1.7	1.0	4	1.38	1.0	$2.9 \times (1, \ldots, 2^8)$
0237−233......	2.32	9.4	3.4	−2	3.53	2.3	$7.0 \times (1, \ldots, 2^8)$
	8.55	3.6	1.2	12	0.47	2.3	$8.1 \times (1, \ldots, 2^5)$
0300+470......	2.32	5.6	4.2	17	0.96	1.0	$2.8 \times (1, \ldots, 2^8)$
	8.55	1.5	1.2	15	0.91	0.6	$1.8 \times (1, \ldots, 2^8)$
0420−014......	2.32	8.0	3.7	2	3.04	1.7	$6.7 \times (1, \ldots, 2^8)$
	8.55	2.2	1.0	2	1.32	1.4	$5.7 \times (1, \ldots, 2^7)$
0430+052......	2.32	7.7	3.5	3	0.98	1.9	$5.6 \times (1, \ldots, 2^7)$
	8.55	2.3	1.0	8	1.17	1.6	$5.5 \times (1, \ldots, 2^7)$
0454−234......	2.32	8.1	3.3	−1	1.89	1.2	$3.7 \times (1, \ldots, 2^8)$
	8.55	2.2	0.9	−1	1.31	1.0	$2.9 \times (1, \ldots, 2^8)$
0552+398......	2.32	6.7	4.5	22	4.08	2.3	$6.9 \times (1, \ldots, 2^9)$
	8.55	1.9	1.2	20	5.09	1.4	$5.0 \times (1, \ldots, 2^9)$
0646−306......	2.32	9.2	3.7	3	0.66	1.2	$3.5 \times (1, \ldots, 2^7)$
	8.55	2.6	1.0	5	0.77	0.9	$2.7 \times (1, \ldots, 2^8)$
0710+439......	2.32	5.7	4.7	34	1.19	1.2	$3.6 \times (1, \ldots, 2^8)$
	8.55	1.7	1.4	57	0.30	1.1	$3.9 \times (1, \ldots, 2^6)$
0727−115......	2.32	8.4	4.0	7	4.41	1.5	$6.1 \times (1, \ldots, 2^9)$
	8.55	2.3	1.1	7	3.56	1.5	$5.8 \times (1, \ldots, 2^9)$
0851+202......	2.32	6.7	4.5	7	2.14	1.1	$3.3 \times (1, \ldots, 2^9)$
	8.55	1.8	1.2	7	1.42	1.0	$3.0 \times (1, \ldots, 2^8)$
0919−260......	2.32	12.4	3.9	13	1.34	1.3	$3.2 \times (1, \ldots, 2^8)$
	8.55	3.4	1.1	13	0.99	0.9	$2.8 \times (1, \ldots, 2^8)$
0953+254......	2.32	6.3	4.6	10	1.57	1.0	$3.0 \times (1, \ldots, 2^9)$
	8.55	1.7	1.3	8	1.20	0.8	$2.7 \times (1, \ldots, 2^8)$
1034−293......	2.32	12.6	4.0	5	1.07	1.7	$5.1 \times (1, \ldots, 2^7)$
	8.55	3.4	1.1	4	1.66	1.2	$3.5 \times (1, \ldots, 2^8)$
1127−145......	2.32	9.3	3.8	7	3.57	2.1	$6.2 \times (1, \ldots, 2^9)$
	8.55	2.6	1.0	6	0.97	1.6	$5.5 \times (1, \ldots, 2^7)$
1156+295......	2.32	6.0	4.3	3	1.00	1.1	$3.3 \times (1, \ldots, 2^8)$
	8.55	1.6	1.2	3	0.98	0.8	$2.5 \times (1, \ldots, 2^8)$
1308+326......	2.32	5.7	4.0	−6	2.34	1.1	$3.2 \times (1, \ldots, 2^9)$
	8.55	1.6	1.1	−7	3.50	1.2	$4.2 \times (1, \ldots, 2^9)$
1313−333......	2.32	8.7	3.3	−3	1.04	1.6	$6.3 \times (1, \ldots, 2^7)$
	8.55	2.6	0.9	0	1.78	2.2	$7.7 \times (1, \ldots, 2^7)$
1323+321......	2.32	6.4	4.8	−3	0.74	1.5	$3.8 \times (1, \ldots, 2^7)$
	8.55	7.7	7.1	38	0.53	2.9	$8.6 \times (1, \ldots, 2^5)$
1334−127......	2.32	8.3	3.5	1	3.47	1.8	$7.2 \times (1, \ldots, 2^8)$
	8.55	2.3	1.0	1	4.37	1.5	$6.1 \times (1, \ldots, 2^9)$
1345+125......	2.32	8.0	4.3	−4	0.51	3.7	$12.8 \times (1, \ldots, 2^5)$
	8.55	2.3	1.0	−7	0.35	1.3	$5.2 \times (1, \ldots, 2^6)$
1404+286......	2.32	6.0	3.8	−4	1.76	1.8	$6.7 \times (1, \ldots, 2^7)$
	8.55	1.6	1.1	−5	1.19	0.9	$3.1 \times (1, \ldots, 2^8)$
1502+106......	2.32	7.2	3.8	−1	1.81	1.2	$3.7 \times (1, \ldots, 2^8)$
	8.55	1.9	1.0	−1	1.38	1.2	$3.6 \times (1, \ldots, 2^8)$
1611+343......	2.32	5.6	3.7	−1	3.38	2.3	$9.1 \times (1, \ldots, 2^8)$
	8.55	1.5	1.0	−2	2.10	1.2	$3.6 \times (1, \ldots, 2^9)$
1622−253......	2.32	9.0	3.4	−2	1.53	1.7	$5.2 \times (1, \ldots, 2^8)$
	8.55	2.5	0.9	−2	1.66	1.9	$7.5 \times (1, \ldots, 2^7)$
1739+522......	2.32	4.6	4.2	−8	0.97	0.8	$2.7 \times (1, \ldots, 2^8)$
	8.55	1.3	1.2	−6	0.52	0.6	$1.7 \times (1, \ldots, 2^8)$
1741−038......	2.32	7.9	3.6	0	2.07	1.2	$3.7 \times (1, \ldots, 2^9)$
	8.55	2.1	1.0	0	2.84	1.2	$4.1 \times (1, \ldots, 2^9)$
1749+096......	2.32	7.2	3.4	−4	1.36	1.2	$3.7 \times (1, \ldots, 2^8)$
	8.55	2.0	0.9	−4	2.71	1.2	$3.5 \times (1, \ldots, 2^9)$
1803+784......	2.32	4.4	3.9	39	1.64	0.9	$2.6 \times (1, \ldots, 2^9)$
	8.55	1.2	1.1	40	1.98	0.9	$2.7 \times (1, \ldots, 2^9)$
1821+107......	2.32	7.3	4.0	−5	1.25	1.0	$3.0 \times (1, \ldots, 2^8)$
	8.55	2.0	1.1	−4	0.49	0.8	$2.3 \times (1, \ldots, 2^7)$
1826+796......	2.32	11.8	4.5	51	0.40	1.0	$2.9 \times (1, \ldots, 2^7)$
	8.55	2.1	1.7	28	0.32	0.6	$1.9 \times (1, \ldots, 2^7)$
1921−293......	2.32	8.2	3.1	−8	10.6	13.5	$53.9 \times (1, \ldots, 2^7)$
	8.55	2.2	0.8	−8	17.3	7.4	$29.5 \times (1, \ldots, 2^9)$

TABLE 1—*Continued*

Source	ν (GHz)	Beam[a] a (mas)	b (mas)	ϕ	Peak (Jy beam^{-1})	rms[b] (mJy beam^{-1})	Contour Levels[c] (mJy beam^{-1})
2021+614......	2.32	4.6	4.3	−88	1.09	1.6	$5.7 \times (1, \ldots, 2^7)$
	8.55	1.2	1.2	−83	1.75	0.9	$3.3 \times (1, \ldots, 2^9)$
2128−123......	2.32	9.1	3.7	−5	1.68	1.7	$5.2 \times (1, \ldots, 2^8)$
	8.55	2.5	1.0	−6	1.45	1.9	$7.8 \times (1, \ldots, 2^7)$
2134+004......	2.32	7.7	3.3	−4	7.64	6.8	$30.7 \times (1, \ldots, 2^7)$
	8.55	2.1	0.9	−4	3.27	4.6	$18.5 \times (1, \ldots, 2^7)$
2145+067......	2.32	7.5	3.4	−1	2.47	3.4	$10.1 \times (1, \ldots, 2^7)$
	8.55	2.1	0.9	−2	7.73	3.9	$15.6 \times (1, \ldots, 2^8)$
2216−038......	2.32	8.0	3.6	−2	2.69	1.7	$5.8 \times (1, \ldots, 2^8)$
	8.55	2.2	1.0	−2	1.57	1.0	$4.1 \times (1, \ldots, 2^8)$
2234+282......	2.32	5.9	3.8	−2	1.60	1.1	$3.3 \times (1, \ldots, 2^8)$
	8.55	1.6	1.0	−2	1.23	0.7	$2.0 \times (1, \ldots, 2^9)$
2255−282......	2.32	7.8	3.1	−2	1.03	1.3	$3.9 \times (1, \ldots, 2^8)$
	8.55	2.3	0.9	−4	1.85	1.0	$3.5 \times (1, \ldots, 2^9)$
2337+264......	2.32	5.9	4.2	−4	0.82	1.0	$2.9 \times (1, \ldots, 2^8)$
	8.55	1.6	1.2	−4	0.32	1.2	$3.6 \times (1, \ldots, 2^6)$

[a] The restoring beam is an elliptical Gaussian with FWHM major axis a and minor axis b, with major axis in position angle ϕ (measured north through east).

[b] The root mean square (rms) of the residuals of the final hybrid image.

[c] Contour levels are represented by the geometric series $1, \ldots, 2^n$; e.g., for $n = 5$ the contour levels would be ± 1, 2, 4, 8, 16, 32.

range at 2.32 GHz is ~3000:1 and is ~3600:1 at 8.55 GHz. The average dynamic range at 2.32 GHz is ~1200:1 and is ~1400:1 at 8.55 GHz. The average rms noise at 2.32 GHz is ~2.0 mJy beam^{-1} and is ~1.5 mJy beam^{-1} at 8.55 GHz. Figure 3 shows the rms noise plotted against the peak of the images for all sources at both 2.32 GHz and 8.55 GHz. Values for three sources (1921−293 at both frequencies, 2134+004 at 2.32 GHz, and 2145+067 at 8.55 GHz) lie outside the plotted range. Figure 3 shows that the rms noise in the images at both frequencies increases only slightly with increasing peak flux density. Most values of the rms noise are less than ~2.5 mJy beam^{-1} at both frequencies. This suggests that we have come close to reaching the thermal noise limit for these sources, a remarkable result considering the variation in (u, v) coverage from source to source. The expected thermal noise is estimated to be ~1 mJy beam^{-1} at both frequencies for a 20 minute observation.

Gaussian models were fitted to the self-calibrated *visibility data* using DIFMAP. Results of the model fitting are listed in Table 2. The last column in this table lists the reduced χ^2 of the fit between the model and the visibility

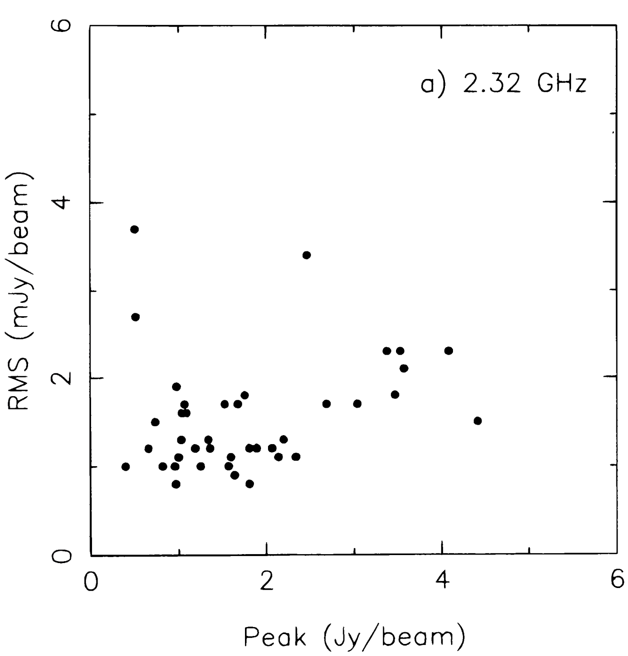

FIG. 3*a*

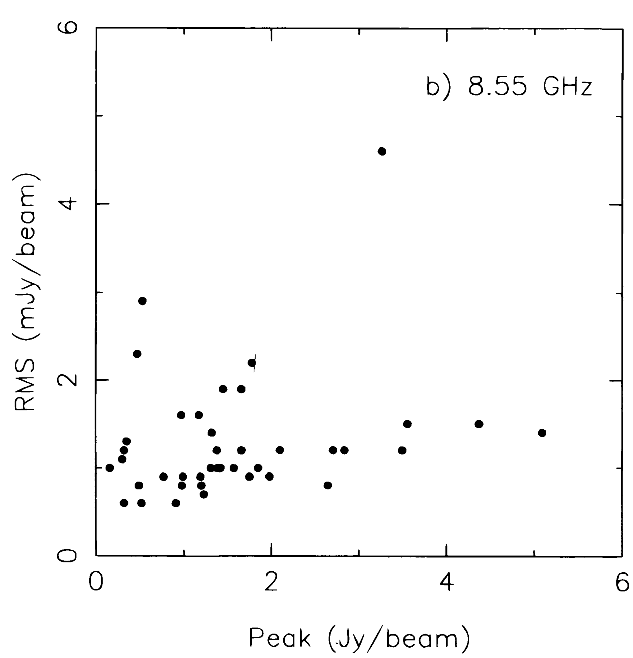

FIG. 3*b*

FIG. 3.—The rms noise plotted against the peak of the images for all sources at (*a*) 2.32 GHz and (*b*) 8.55 GHz. Values for three sources (1921−293 at both frequencies, 2134+004 at 2.32 GHz, and 2145+067 at 8.55 GHz) lie outside the plotted range.

TABLE 2

Gaussian Models[a]

Source	ν (GHz)	Component	S (Jy)	r (mas)	θ	a (mas)	b/a	ϕ	χ^2
0056−001......	2.32	1	0.80	0.0	...	5.04	0.69	−17°	1.05
		2	0.40	8.1	153	4.77	0.23	−30	
		3	0.46	15.6	−22	18.78	1.00	...	
	8.55	1	0.19	0.0	...	0.56	0.56	−20	1.08
		2	0.37	8.0	−32	7.95	1.00	...	
0212+735......	2.32	1	1.57	0.0	...	1.46	0.00	−78	1.05
		2	0.52	2.0	102	0.79	0.81	−28	
		3	0.29	5.5	101	3.26	0.40	−85	
		4	0.57	13.3	91	2.81	0.62	−62	
		5	0.02	41.1	95	4.93	1.00	...	
	8.55	1	2.59	0.0	...	0.33	0.35	−33	1.07
		2	0.29	0.6	127	0.48	1.00	...	
		3	0.30	2.1	104	1.70	0.39	−67	
		4	0.04	6.4	104	1.56	1.00	...	
		5	0.10	14.0	92	1.94	1.00	...	
0234+285......	2.32	1	1.78	0.0	...	1.66	0.00	−16	0.85
		2	1.10	3.5	−9	3.20	0.62	2	
		3	0.11	12.1	3	5.81	1.00	...	
	8.55	1	1.32	0.0	...	0.48	0.00	−22	0.92
		2	0.30	1.0	−10	0.61	1.00	...	
		3	0.26	2.9	−17	1.39	1.00	...	
		4	0.24	5.1	−7	2.20	1.00	...	
0237−233......	2.32	1	3.91	0.0	...	3.17	0.24	38	1.37
		2	0.69	3.3	86	2.69	1.00	...	
		3	0.86	3.4	−136	2.33	1.00	...	
		4	0.77	10.0	−132	1.38	0.51	57	
	8.55	1	0.74	0.0	...	2.54	0.42	29	1.44
		2	0.09	3.3	73	2.76	1.00	...	
		3	0.30	2.6	−132	1.64	1.00	...	
		4	0.57	10.1	−130	1.16	0.00	62	
0300+470......	2.32	1	0.95	0.0	...	1.57	0.09	−37	0.88
		2	0.14	2.6	109	2.13	1.00	...	
		3	0.05	6.4	128	5.88	1.00	...	
	8.55	1	0.89	0.0	...	0.21	0.45	−36	0.84
		2	0.12	1.0	152	0.26	1.00	...	
		3	0.05	1.5	148	0.74	1.00	...	
		4	0.05	3.0	114	2.62	1.00	...	
0420−014......	2.32	1	3.10	0.0	...	0.93	0.64	−17	0.98
		2	0.09	13.9	179	6.44	1.00	...	
	8.55	1	1.19	0.0	...	0.60	0.46	0	0.99
		2	0.42	1.1	−147	0.36	1.00	...	
		3	0.45	1.7	−177	0.77	1.00	...	
0430+052......	2.32	1	0.94	0.0	...	1.61	0.00	67	1.03
		2	0.64	3.7	−100	3.57	0.00	73	
		3	0.65	8.8	−106	2.42	1.00	...	
		4	0.26	12.2	−106	2.58	1.00	...	
		5	0.10	20.3	−104	5.99	1.00	...	
		6	0.08	45.9	−97	12.82	1.00	...	
		7	0.15	83.9	−100	5.32	1.00	...	
	8.55	1	1.60	0.0	...	1.14	0.10	64	1.05
		2	0.17	2.2	−101	3.14	0.00	83	
		3	0.14	4.9	−103	1.27	1.00	...	
		4	0.03	7.4	−99	0.32	1.00	...	
		5	0.21	9.5	−106	2.18	1.00	...	
		6	0.07	12.6	−105	2.32	1.00	...	
0454−234......	2.32	1	2.02	0.0	...	1.56	0.45	48	1.19
		2	0.06	5.0	−128	2.82	1.00	...	
	8.55	1	1.09	0.0	...	0.29	0.00	−29	1.01
		2	0.51	0.8	151	0.85	1.00	...	
0552+398......	2.32	1	4.24	0.0	...	1.25	0.52	−60	0.98
	8.55	1	4.85	0.0	...	0.44	0.84	86	0.99
		2	1.27	0.7	−71	0.68	1.00	...	
0646−306......	2.32	1	0.58	0.0	...	1.05	0.00	83	1.37
		2	0.28	2.4	99	1.61	1.00	...	
	8.55	1	0.78	0.0	...	0.19	0.00	−82	1.17
		2	0.17	2.1	93	2.38	1.00	...	
0710+439......	2.32	1	1.05	0.0	...	1.48	0.62	−58	0.93
		2	0.43	1.6	−129	6.79	0.39	−45	
		3	0.73	8.2	178	1.96	0.00	0	
		4	0.30	23.7	−179	1.38	0.62	2	

Source	ν (GHz)	Component	S (Jy)	r (mas)	θ	a (mas)	b/a	ϕ	χ^2
		5	0.03	22.8	168	4.86	1.00	...	
	8.55	1	0.52	0.0	...	2.21	0.22	6	1.20
		2	0.12	8.2	−6	2.87	0.02	−71	
		3	0.33	9.0	−1	0.75	0.50	85	
		4	0.11	15.2	−178	1.20	1.00	...	
0727−115......	2.32	1	4.48	0.0	...	1.10	0.00	−67	1.44
		2	0.37	4.6	−40	8.09	1.00	...	
	8.55	1	3.69	0.0	...	0.39	0.56	87	1.26
		2	0.42	1.1	−66	2.72	0.24	−39	
0851+202......	2.32	1	2.18	0.0	...	1.18	0.00	75	0.86
		2	0.10	4.1	−116	2.21	1.00	...	
		3	0.04	10.7	−119	6.44	1.00	...	
	8.55	1	1.15	0.0	...	0.38	0.00	−89	1.00
		2	0.70	0.8	−93	0.92	0.28	81	
		3	0.05	2.8	−108	2.31	1.00	...	
		4	0.01	7.6	−123	1.35	1.00	...	
0919−260......	2.32	1	1.82	0.0	...	3.68	0.51	−79	1.24
		2	0.18	4.8	−65	4.28	1.00	...	
		3	0.02	14.2	−65	4.04	1.00	...	
	8.55	1	0.95	0.0	...	0.56	0.71	83	1.05
		2	0.43	0.8	−83	0.83	1.00	...	
		3	0.06	4.3	−61	4.48	1.00	...	
0953+254......	2.32	1	1.57	0.0	...	0.56	0.00	80	0.85
		2	0.04	8.0	−91	7.48	0.00	−89	
	8.55	1	1.38	0.0	...	0.71	0.53	43	0.90
1034−293......	2.32	1	1.05	0.0	...	0.58	0.00	−57	1.34
		2	0.11	3.0	133	1.70	0.00	−13	
		3	0.02	13.8	147	1.71	1.00	...	
		4	0.02	24.0	135	4.40	1.00	...	
	8.55	1	1.74	0.0	...	0.35	0.00	−63	1.16
		2	0.07	2.3	141	0.92	1.00	...	
		3	0.01	5.1	140	0.64	1.00	...	
1127−145......	2.32	1	3.27	0.0	...	1.83	0.27	55	1.22
		2	1.09	3.0	−98	2.14	0.00	46	
		3	1.04	5.3	41	7.69	0.24	49	
		4	0.06	11.2	64	2.96	1.00	...	
		5	0.10	16.2	56	2.36	1.00	...	
		6	0.07	23.2	56	6.29	1.00	...	
		7	0.05	63.3	68	13.00	1.00	...	
	8.55	1	0.97	0.0	...	0.53	0.00	88	1.34
		2	0.37	1.0	85	1.87	0.18	79	
		3	1.02	3.7	83	1.31	0.70	41	
		4	0.08	5.4	74	1.01	1.00	...	
		5	0.13	9.3	56	3.95	1.00	...	
1156+295......	2.32	1	0.94	0.0	...	2.11	0.18	−9	0.79
		2	0.31	3.5	14	2.14	1.00	...	
		3	0.24	9.0	33	6.71	1.00	...	
	8.55	1	1.00	0.0	...	0.34	0.26	−11	0.84
		2	0.14	2.5	−5	1.58	1.00	...	
		3	0.08	4.8	16	2.37	1.00	...	
1308+326......	2.32	1	2.32	0.0	...	0.00	1.00	...	0.83
		2	0.22	5.4	−79	3.71	0.55	61	
		3	0.02	12.9	−83	5.33	1.00	...	
	8.55	1	3.11	0.0	...	0.27	0.38	−22	0.89
		2	0.58	0.4	−27	0.39	1.00	...	
		3	0.05	5.5	−75	3.43	1.00	...	
1313−333......	2.32	1	1.06	0.0	...	1.25	0.40	7	1.43
		2	0.25	4.7	−68	3.20	1.00	...	
	8.55	1	1.81	0.0	...	0.34	0.00	−21	1.35
		2	0.04	0.9	−69	0.47	1.00	...	
		3	0.09	4.5	−68	3.41	1.00	...	
1323+321......	2.32	1	0.53	0.0	...	3.60	0.67	−30	1.17
		2	0.97	3.4	170	12.75	1.00	...	
		3	0.75	3.7	71	6.71	1.00	...	
		4	0.27	13.2	120	10.24	1.00	...	
		5	0.14	45.2	127	6.38	1.00	...	
		6	0.35	52.2	140	9.20	1.00	...	
		7	0.52	52.4	129	5.90	1.00	...	
		8	0.82	57.0	130	6.26	0.51	40	
	8.55	1	0.78	0.0	...	5.89	0.86	−44	0.76
		2	0.38	54.0	130	7.50	0.58	−25	

1996ApJS..105..299F

TABLE 2—*Continued*

Source	ν (GHz)	Component	S (Jy)	r (mas)	θ	a (mas)	b/a	ϕ	χ^2
1334−127......	2.32	1	3.45	0.0	...	1.59	0.00	−7	1.23
		2	0.17	2.9	149	0.87	1.00	...	
		3	0.02	9.6	144	0.77	1.00	...	
		4	0.02	27.0	148	3.79	1.00	...	
	8.55	1	4.27	0.0	...	0.51	0.00	−30	1.34
		2	0.58	0.8	155	0.40	1.00	...	
		3	0.10	3.3	165	0.72	1.00	...	
1345+125......	2.32	1	0.53	0.0	...	5.78	0.24	−1	1.99
		2	0.44	9.2	13	4.34	1.00	...	
		3	2.50	12.4	−159	21.69	0.73	19	
		4	0.19	15.2	−5	3.00	1.00	...	
		5	0.43	23.9	−144	6.26	0.46	−32	
		6	0.28	28.1	−18	3.78	1.00	...	
		7	0.52	39.3	−21	4.66	1.00	...	
		8	0.19	48.5	−20	5.18	0.00	−17	
		9	0.13	72.4	−23	5.75	1.00	...	
	8.55	1	0.48	0.0	...	1.60	0.31	−19	0.96
		2	0.33	9.2	162	2.84	0.34	−42	
		3	0.14	19.7	155	4.51	1.00	...	
		4	0.09	43.8	155	1.86	1.00	...	
		5	0.05	51.6	161	1.19	1.00	...	
		6	0.12	65.4	177	3.52	1.00	...	
1404+286......	2.32	1	1.96	0.0	...	1.84	0.78	−10	0.84
		2	0.07	7.0	−125	1.65	0.00	6	
	8.55	1	1.35	0.0	...	0.68	0.66	−10	0.86
		2	0.32	1.3	−20	0.66	1.00	...	
		3	0.09	6.5	−126	1.19	1.00	...	
		4	0.05	7.5	−116	0.21	1.00	...	
1502+106......	2.32	1	1.64	0.0	...	0.95	0.13	−44	0.83
		2	0.30	1.7	119	1.55	1.00	...	
		3	0.17	6.6	81	5.29	1.00	...	
		4	0.02	8.9	140	1.31	1.00	...	
	8.55	1	1.38	0.0	...	0.45	0.22	−39	0.86
		2	0.24	0.9	126	0.55	1.00	...	
		3	0.11	2.0	134	0.97	1.00	...	
		4	0.11	3.0	97	5.72	1.00	...	
1611+343......	2.32	1	4.16	0.0	...	2.98	0.50	−20	1.46
	8.55	1	2.14	0.0	...	0.38	0.00	−9	1.04
		2	0.35	1.5	−178	0.47	1.00	...	
		3	0.65	2.6	172	0.98	1.00	...	
		4	0.37	3.3	156	1.34	1.00	...	
1622−253......	2.32	1	1.67	0.0	...	1.88	0.40	41	1.30
		2	0.04	8.7	−34	3.17	1.00	...	
	8.55	1	1.70	0.0	...	0.39	0.00	31	1.23
		2	0.13	1.8	6	1.73	1.00	...	
1739+522......	2.32	1	0.94	0.0	...	1.19	0.77	31	0.85
		2	0.14	2.0	−20	1.81	1.00	...	
		3	0.04	7.7	28	9.15	1.00	...	
	8.55	1	0.44	0.0	...	0.22	0.08	−24	0.88
		2	0.25	0.7	36	1.35	1.00	...	
		3	0.04	2.4	−10	1.92	1.00	...	
1741−038......	2.32	1	2.09	0.0	...	0.51	1.00	...	0.94
		2	0.04	9.0	172	6.30	1.00	...	
	8.55	1	2.24	0.0	...	0.00	1.00	...	0.93
		2	0.75	0.3	−169	0.55	1.00	...	
1749+096......	2.32	1	1.37	0.0	...	1.06	0.00	54	0.76
		2	0.10	3.1	30	0.53	1.00	...	
		3	0.05	7.8	34	4.37	1.00	...	
	8.55	1	2.73	0.0	...	0.18	0.47	28	0.86
		2	0.11	2.0	26	1.56	1.00	...	
1803+784......	2.32	1	1.63	0.0	...	1.37	0.00	87	1.06
		2	0.34	4.0	−94	7.24	0.28	81	
		3	0.28	27.6	−105	12.11	1.00	...	
	8.55	1	1.91	0.0	...	0.19	0.63	−81	1.03
		2	0.38	1.0	−92	1.53	0.28	83	
		3	0.05	3.5	−86	1.26	1.00	...	
		4	0.05	6.6	−95	2.57	1.00	...	
1821+107......	2.32	1	1.29	0.0	...	1.60	0.14	−24	0.87
		2	0.05	12.4	−1	3.42	1.00	...	
		3	0.04	28.7	−9	8.55	1.00	...	
	8.55	1	0.50	0.0	...	0.79	0.00	−19	0.80

TABLE 2—*Continued*

Source	ν (GHz)	Component	S (Jy)	r (mas)	θ	a (mas)	b/a	ϕ	χ^2
		2	0.18	1.6	−15	0.40	1.00	...	
		3	0.03	2.5	−20	0.51	1.00	...	
1826+796......	2.32	1	0.40	0.0	...	2.78	0.11	55	0.68
		2	0.02	12.6	75	2.81	1.00	...	
		3	0.06	12.8	−117	3.80	1.00	...	
		4	0.07	13.6	63	1.66	0.00	58	
	8.55	1	0.31	0.0	...	0.49	0.80	0	0.78
		2	0.06	1.0	−20	0.17	1.00	...	
		3	0.01	1.2	−108	0.58	0.00	27	
		4	0.01	6.6	−110	1.10	1.00	...	
		5	0.03	11.7	−111	1.34	1.00	...	
		6	0.01	13.9	−118	0.33	1.00	...	
		7	0.11	15.7	−116	0.82	1.00	...	
2021+614......	2.32	1	0.78	0.0	...	1.44	0.55	57	1.14
		2	0.65	2.7	66	1.13	1.00	...	
		3	0.09	6.2	53	4.44	1.00	...	
		4	0.34	5.4	−174	2.12	1.00	...	
		5	0.89	5.8	−149	2.70	0.44	51	
		6	0.06	11.7	143	4.17	1.00	...	
	8.55	1	1.31	0.0	...	0.39	0.54	−10	0.93
		2	0.76	0.4	45	0.58	1.00	...	
		3	0.12	1.7	38	1.27	1.00	...	
		4	0.06	3.2	32	0.38	1.00	...	
		5	0.74	7.0	33	0.55	0.95	30	
		6	0.09	7.7	34	0.70	1.00	...	
		7	0.04	9.7	41	0.72	1.00	...	
2128−123......	2.32	1	1.74	0.0	...	2.15	0.00	29	1.12
		2	0.18	4.0	−149	0.56	0.00	31	
		3	0.19	8.6	−149	1.72	1.00	...	
		4	0.07	16.8	−148	4.04	1.00	...	
		5	0.06	32.7	−148	8.56	1.00	...	
	8.55	1	1.75	0.0	...	1.12	0.00	31	1.49
		2	0.37	1.3	−155	0.82	0.00	−18	
		3	0.14	2.5	−145	1.06	1.00	...	
		4	0.10	5.0	−150	1.18	1.00	...	
2145+067......	2.32	1	2.46	0.0	...	1.12	0.00	−52	1.05
		2	0.81	5.2	135	6.64	0.08	−28	
		3	0.17	73.9	161	5.02	1.00	...	
		4	0.17	59.9	155	12.04	1.00	...	
	8.55	1	6.34	0.0	...	0.36	0.39	−40	1.40
		2	2.54	0.5	128	0.58	0.30	−51	
		3	0.03	2.8	130	0.69	0.00	−16	
		4	0.06	6.8	135	5.42	0.03	−25	
2216−038......	2.32	1	2.75	0.0	...	1.51	0.00	23	1.07
		2	0.02	11.4	−163	1.31	1.00	...	
	8.55	1	1.20	0.0	...	0.47	0.49	16	0.88
		2	0.86	1.2	−173	0.45	1.00	...	
2234+282......	2.32	1	1.68	0.0	...	1.27	0.00	68	0.91
	8.55	1	1.27	0.0	...	0.46	0.25	49	0.88
		2	0.20	0.9	−97	1.04	1.00	...	
2255−282......	2.32	1	0.95	0.0	...	1.04	0.00	33	1.31
		2	0.41	3.2	−137	1.09	1.00	...	
		3	0.07	4.7	25	1.05	1.00	...	
		4	0.04	8.0	−126	2.80	1.00	...	
		5	0.04	14.7	−121	2.93	1.00	...	
	8.55	1	1.89	0.0	...	0.18	0.70	54	1.08
		2	0.09	2.2	−141	0.81	1.00	...	
		3	0.12	3.9	−138	1.15	1.00	...	
2337+264......	2.32	1	1.14	0.0	...	4.10	0.24	−63	0.95
		2	0.30	7.4	104	0.92	0.64	−17	
	8.55	1	0.36	0.0	...	0.49	0.73	86	0.89
		2	0.14	6.0	−78	1.65	0.38	−87	
		3	0.20	8.6	−74	2.01	0.41	−86	

[a] The models fitted to the visibility data are of Gaussian form with flux density S and FWHM major axis a and minor axis b, with major axis in position angle ϕ (measured north through east). Components are separated from the (arbitrary) origin of the image by an amount r in position angle θ, which is the position angle (measured north through east) of a line joining the components with the origin.

data. The two sources 1921 − 293 and 2134 + 004 were too complex to model with the available data and are not included in Table 2. The reduced χ^2 has an expected value of 1.0 (however, when the data are self-calibrated, the number of degrees of freedom is reduced so that the expected value of the reduced χ^2 may actually be significantly less than 1.0; see Henstock et al. 1995).

Although the agreement between the fitted models and the data is not as good as that produced by the hybrid images (models with many CLEAN components), inspection of plots of residuals in the image plane, after subtracting the Gaussian models from the visibility data, revealed that the Gaussian models generally describe the visibility data quite well with typical residuals of $\sim 10\ \sigma$. However, because of incomplete sampling in the (u, v) plane, these models may not be unique. They represent only one *possible* deconvolution of complex source structure. Such deconvolutions can be misleading.

4. DISCUSSION

The variation of intrinsic structure from source to source in our sample ranges from relatively compact naked-core objects such as 0552 + 398 and 1741 − 038, to compact double/triple sources such as 0710 + 439 and 2021 + 614, to complex core-jet objects such as 0430 + 052 and 2138 − 123. Many of the sources have dominant cores containing the majority of the total flux density and angular sizes less than several milliarcseconds. However, at some level, almost all the observed sources show structure characteristic of a core-jet morphology, often with multiple jet components. Figure 4 shows the distribution of the ratio of 8.55 GHz core component flux density to 8.55 GHz total source flux density, where the flux density values have been taken from the fitted models listed in Table 2. The median and mean flux density ratios are 0.73 and 0.70, respectively, showing that for about half the sources the core component contains more than 70% of the total flux density. Sources with dominant cores are known to be highly variable, both spatially and temporally.

Many of the more complex sources have shown inconsistencies in their derived astrometric positions when examined on an epoch-by-epoch basis (Johnston et al. 1995;

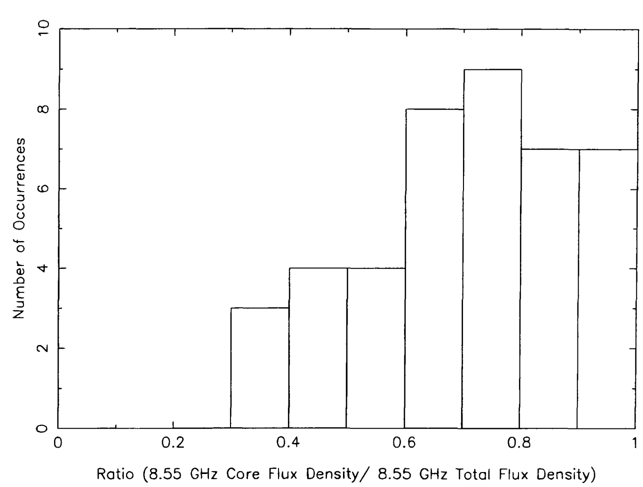

FIG. 4.—The distribution of the ratio of 8.55 GHz core component flux density to 8.55 GHz total source flux density for all sources. The flux density values were taken from the fitted models listed in Table 2.

Eubanks et al. 1996). Charlot (1990) has modeled the effects of radio source structure on measured VLBI group delays and delay rates. Results of this modeling suggest that these effects can be significant (typically at a level of 100 ps [~ 3 cm at the surface of the Earth ~ 1 mas] in the group delay). For a simple two-component source model, numerical simulations show that the closer the flux densities of the two components are, the larger the structure effects become (Charlot 1990). Structure corrections based on the images presented here have been calculated and applied to the Jet Propulsion Laboratory's (JPL) geodetic/astrometric database. Over half the observations in the JPL database are of one of these 42 sources. Results of these calculations (O. J. Sovers 1995, private communication) confirm that intrinsic structure contributions to the measured group delay can be significant, with corrections as large as ~ 1.5 ns. The average of the calculated group delay corrections exceeded 10 ps for 16 of the 42 sources, while the maximum group delay correction for any of the 42 sources was always greater than 10 ps. Analysis of these results in terms of quantifying their effect on precise position determination is underway and will be reported elsewhere.

Some of the more well-known sources in our sample have been observed heavily by others. However, the majority of the reference frame sources have never been imaged, either with sufficient sensitivity, sufficient resolution, or at these frequencies. Of the sources reported by Johnston et al. (1995) (this includes sources in the range $\alpha = 0^h$–24^h, $\delta = -90°$ to $+90°$, inclusive), we estimate that imaging observations exist for $\lesssim 25\%$. These include observations concentrating on individual sources together with several of the large Northern Hemisphere VLBI surveys (Pearson & Readhead 1981, 1988; Taylor et al. 1994; Henstock et al. 1995), which have concentrated on high declination sources, and Southern Hemisphere surveys (Preston et al. 1989), which have lacked the spatial frequency coverage and resolution to image sources on sub-milliarcsecond scales. More images are undoubtedly available, but they are few and far between. More importantly, the majority of previous VLBI observations have been carried out at frequencies other than those used to do precise astrometry. Few observations or surveys of extragalactic sources have been carried out at either 2 GHz or 8 GHz. For reference frame use, extrapolation or interpolation of source structure from other frequencies and resolutions would produce effective position errors, especially when complex, variable structure is present and without current spectral information. In order to quantify accurately errors introduced by intrinsic source structure, high-quality images obtained *at the same frequencies* as those used for astrometry are required *for each source.*

5. SUMMARY

The advent of the VLBA telescope has allowed snapshot imaging of extragalactic radio sources with sensitivities obtained previously only with full-synthesis observations. In addition, the dual-frequency 2 GHz and 8 GHz system allows simultaneous observations in two widely separated frequency bands, with application to geodetic and astrometric work as well as to imaging. Surveys of large numbers of sources can now be done routinely and often. This has particular application to monitoring radio reference frame sources for changes in intrinsic structure. Many of the sources presented here have dominant cores containing the majority of the total flux density. Sources with dominant cores are known to be highly variable, both spatially and temporally. Frequent observations of the radio reference frame sources are therefore necessary to determine the level at which source structure variation, such as superluminal motion, will affect the long-term stability and accuracy of the radio reference frame.

The authors would like to thank Tim Pearson for helpful comments on the manuscript.

REFERENCES

Charlot, P. 1990, AJ, 99, 1309
Clegg, A. W., Fey, A. L., & Fiedler, R. L. 1996, ApJ, 457, L23
Eubanks, T. M., et al. 1996, in IAU Symp. 166, Secular Motions of Extragalactic Radio Sources and the Stability of the Radio Reference Frame, The Hague, in press
Fiedler, R., Dennison, B., Johnston, K. J., Waltman, E. B., & Simon, R. S. 1994, ApJ, 430, 581
Henstock, D. R., Browne, I. W. A., Wilkinson, P. N., Taylor, G. B., Vermeulen, R. C., Pearson, T. J., & Readhead, A. C. S. 1995, ApJS, 100, 1
Johnston, K. J., et al. 1995, AJ, 110, 880
Napier, P. J., Bagri, D. S., Clark, B. G., Rogers, A. E. E., Romney, J. D., Thompson, A. R., & Walker, R. C. 1994, Proc. IEEE, 82, 658
Pearson, T. J., & Readhead, A. C. S. 1981, ApJ, 248, 61
———. 1984, ARA&A, 22, 97
———. 1988, ApJ, 328, 114
Preston, R. A., et al. 1989, AJ, 98, 1
Rogers, A. E. E. 1970, Radio Sci., 5, 1239
Shepherd, M. C., Pearson, T. J., & Taylor, G. B. 1995, BAAS, 27, 903
Taylor, G. B., Vermeulen, R. C., Pearson, T. J., Readhead, A. C. S., Henstock, D. R., Browne, I. W. A., & Wilkinson, P. N. 1994, ApJS, 95, 345
Wehrle, A. E., Cohen, M. H., & Unwin, S. C. 1990, ApJ, 351, L1